
MOX-Report No. 05/2023

# Novel approaches for the numerical solution of fluid-structure interaction in the aorta

Fumagalli, I.; Vergara, C.

MOX, Dipartimento di Matematica
Politecnico di Milano, Via Bonardi 9 - 20133 Milano (Italy)

mox-dmat@polimi.it https://mox.polimi.it

# Novel Approaches for the Numerical Solution of Fluid-Structure Interaction in the Aorta

Ivan Fumagalli[1], Christian Vergara[2]

[1] MOX, Dipartimento di Matematica, Politecnico di Milano
[2] LABS, Dipartimento di Chimica, Materiali e Ingegneria Chimica "Giulio Natta", Politecnico di Milano

**ABSTRACT**

The aorta is the artery that undergoes the most deformation during the heartbeat. This is associated with the strong Fluid-Structure Interaction (FSI) occurring between the blood flow and the aortic wall. Moreover, also the dynamics of the aortic valve is the result of a FSI process. In this work, we describe the mathematical formulation of both vascular and valve FSI problems and we review the most recent numerical strategies for their solution. Concerning vascular FSI, we consider a moving-domain approach encompassing an arbitrary Lagrangian-Eulerian formulation of the fluid equations, which is the most employed framework in hemodynamics applications. In this context, we provide a systematic description and comparison of different algorithms for the coupling between the fluid and the structure model. In terms of valve FSI, we report a survey on the different numerical methods for the treatment of surfaces immersed and moving in a fluid, with particular focus on unfitted methods, which are the most established for cardiac valve modeling, and the more recent promising family of Cut Finite Elements methods. Aiming to point out the main difficulties specifically related to aortic FSI simulation in a patient-specific context, we also review strategies for the imposition of boundary conditions, the recovery of a zero-pressure configuration of the vessel wall, and the calibration and validation of computational models against clinical data.

**KEYWORDS**

Finite Element Method, Partitioned schemes, Monolithic schemes, Arbitrary Lagrangian-Eulerian, Immersed Boundary/Fictitious Domain Method, Unfitted methods

## 1 INTRODUCTION & MOTIVATIONS

The aorta is the most deformable vessel among the arteries, experiencing a change of cross-section area of up to about 30%, corresponding to a change of radius of up to about 15% [5]. This is due to the large amount of elastin and to the high blood pressure, and its ultimate goal is to store about 50% of incoming blood during systole. This blood supply is then released during diastole thanks to the vessel wall elastic response (*Windkessel effect*), ensuring an almost constant exchange of oxygen with the tissues [190]. In what follows, we will refer to this *Fluid-Structure Interaction* (FSI) mechanism arising between blood and vessel wall as *vascular FSI*.

For the reasons above, a FSI modeling is required to describe the mechanics of the aorta, whenever the attention is on structural quantities (such as Von Mises stresses) to assess, e.g., plaque and aneurysm rupture risk, or on local blood dynamics features that could be heavily influenced by FSI and wall movement, such as in presence of dissections or when a Thoracic Endovascular Aortic Repair (TEVAR) procedure is performed.

This is in accordance with the great amount of aortic studies that considered FSI in the last decade. We mention for example works on: the blood dynamics in the ascending aorta in presence of a Transcatheter Aortic Valve Replacement/Implantation (TAVR/TAVI) [132], the effect of hemodynamics on TEVAR implant [151, 156, 18, 2, 146], the influence of blood flow on stress in thoracic aneurysms [43], the hemodynamics in presence of aortic dissection [157, 19, 49].

We are interested here in describing also another FSI mechanism occurring in the aorta, namely the interaction between blood and aortic valve leaflets. The valve is an immersed thin structure experiencing large displacements during closure-opening phases (up to 100% of the leaflet dimension) and contact among leaflets. We will refer to this mechanism as *valve FSI*.

The requirement of a FSI modeling (although in general different from the vascular case) is here mandatory in order to well describe the large valve displacements [137]. Recent works on this topic carry out investigations on valvular pathologies – such as bicuspid aortic valve [62] or aortic valve stenosis [131, 117] – and treatments – e.g., surgical repairment [64] or transcatheter aortic valve implantation [132, 197, 85, 20].

A representative example of aortic blood velocity obtained with both vascular and valve FSI is reported in Fig. 1.

## 2 THE MATHEMATICAL PROBLEM FOR VASCULAR FSI

The most standard and used formulation for vascular FSI is based on an *Arbitrary Lagrangian-Eulerian* (ALE) description of fluid equations [100, 60], in combination with a Lagrangian description[1] of the structure problem. The ALE

1. Quantities referred to a Lagrangian description will be indicated with $\widehat{\ }$

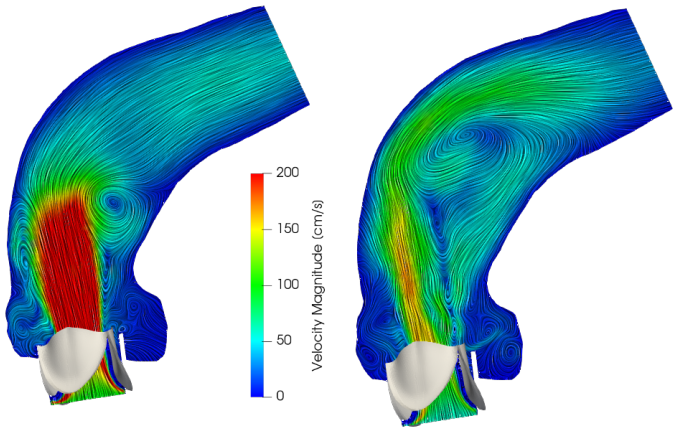


**FIGURE 1** Blood velocity field of a TAVR/TAVI patient on a slice of the ascending aorta, at systolic peak (left) and in the systolic deceleration phase (right). Vascular FSI is solved by an ALE-based monolithic method (see Section 3) and coupled with the valve leaflets via the RIIS method (see Section 4.3). Code: `life`$^{\text{x}}$ - `https://lifex.gitlab.io`. Credits: A. Castorio & B. Loretoni.

formulation consists in extending the physical displacement at the fluid-structure interface in the whole fluid domain, associating a virtual fluid domain displacement $\boldsymbol{d}_f$, and in writing the Navier-Stokes equations in a frame of reference which moves according to such displacement. To this aim, the Reynolds transport formula is used to express the ALE material time derivative $\frac{\delta}{\delta t}$ of a vectorial function $\boldsymbol{v}$ in terms of the Eulerian one:

$$\frac{\delta \boldsymbol{v}}{\delta t} = \frac{\partial \boldsymbol{v}}{\partial t} + \boldsymbol{u}_f \cdot \nabla \boldsymbol{v},$$

where $\boldsymbol{u}_f = \frac{\partial \boldsymbol{d}_f}{\partial t}$ is the fluid domain velocity.

To obtain the virtual fluid domain displacement $\boldsymbol{d}_f$ an extra problem is solved, usually a harmonic extension[2] of the FS interface displacement. The fluid domain displacement $\boldsymbol{d}_f$ is then used to move the points of the fluid mesh accordingly, obtaining the new computational fluid domain[3].

Thus, the FSI problem reads:
Find the fluid velocity $\boldsymbol{u}$, the fluid pressure $p$, the fluid domain displacement $\boldsymbol{d}_f$,

2. Other choices considered so far are linear elasticity [175], biharmonic extension [199], and incremental extensions [171]. In all the cases, the aim is to improve regularity of the fluid mesh motion avoiding distortion of the elements
3. Usually, the extension problem is solved in a Lagrangian framework, thus the update of the fluid domain is performed with respect to the reference position: $\boldsymbol{x}(t) = \widehat{\boldsymbol{x}} + \widehat{\boldsymbol{d}}_f(t, \widehat{\boldsymbol{x}})$

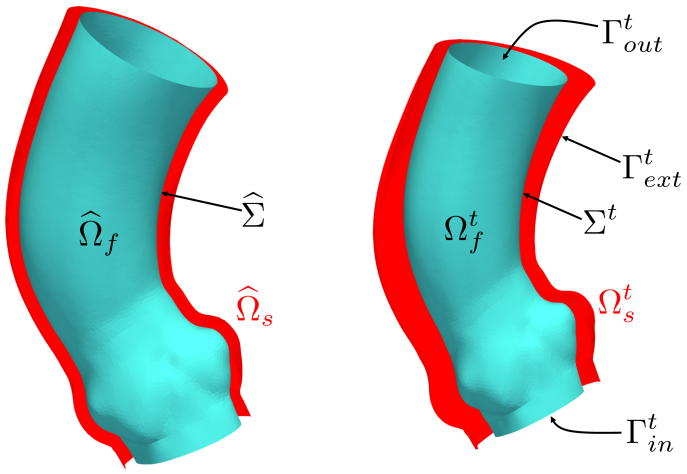


**FIGURE 2** Domains and boundaries of the FSI problem: in blue the fluid domain and in red the structure domain. Left: reference configuration; right: current configuration at time $t$.

and the structure displacement $\boldsymbol{d}$, such that

$$\rho_f \left( \frac{\delta \boldsymbol{u}}{\delta t} + (\boldsymbol{u} - \boldsymbol{u}_f) \cdot \nabla \boldsymbol{u} \right) - \nabla \cdot \boldsymbol{T}_f(\boldsymbol{u}, p) = \boldsymbol{0} \qquad \text{in } \Omega^t_f, \qquad (1a)$$

$$\nabla \cdot \boldsymbol{u} = 0 \qquad \text{in } \Omega^t_f, \qquad (1b)$$

$$\boldsymbol{u} = \frac{\partial \boldsymbol{d}}{\partial t} \qquad \text{on } \Sigma^t, \qquad (1c)$$

$$\boldsymbol{T}_s(\boldsymbol{d})\boldsymbol{n} = \boldsymbol{T}_f(\boldsymbol{u}, p)\boldsymbol{n} \qquad \text{on } \Sigma^t, \qquad (1d)$$

$$\rho_s \frac{\partial^2 \widehat{\boldsymbol{d}}}{\partial t^2} - \nabla \cdot \widehat{\boldsymbol{T}}_s \left( \widehat{\boldsymbol{d}} \right) = \boldsymbol{0} \qquad \text{in } \widehat{\Omega}_s, \qquad (1e)$$

$$\widehat{\boldsymbol{d}}_f = \widehat{\boldsymbol{d}} \qquad \text{on } \widehat{\Sigma}, \qquad (1f)$$

$$-\triangle \widehat{\boldsymbol{d}}_f = \boldsymbol{0} \qquad \text{in } \widehat{\Omega}_f, \qquad (1g)$$

where $\Omega^t_f$ and $\Omega_s$ are the fluid and structure domains represented in Fig. 2, $\rho_f$ and $\rho_s$ the densities, $\boldsymbol{T}_f = -p\boldsymbol{I} + \mu \left( \nabla \boldsymbol{u} + (\nabla \boldsymbol{u})^T \right)$ the fluid Cauchy stress tensor with $\mu$ the viscosity[4], and $\boldsymbol{T}_s$ is the first Piola-Kirchhoff tensor corresponding to a constitutive law based on Finite Elasticity, suitable for the arterial vessel, see [101]. Conditions (1c)-(1d) represent the no-slip and third Newton law continuity interface conditions, referred to as *kinematic* and *dynamic* conditions, respectively. Condition (1f) represents the geometric condition, which in fact couples the fluid and the structure also from the geometric point of view. System

4. For the aorta, often a Newtonian model is considered. However, what follows could be applied to the non-Newtonian case as well [157]

(1) needs to be supplemented with suitable initial conditions for $\boldsymbol{u}$, $\boldsymbol{d}$, $\dot{\boldsymbol{d}}$ and boundary conditions on $\partial\Omega_j \setminus \Sigma$, $j = f, s$. Finally, notice the zero forcing terms both for the fluid and the structure problems, due to the negligible action of gravity and other external forces on the aorta system.

An alternative strategy, not detailed here, is the *fully Eulerian* formulation proposed in [162] where both the fluid and structure subproblems are written in an Eulerian framework, allowing to avoid artificial fluid domain mapping as in the ALE formulation.

## 3 NUMERICAL APPROACHES FOR VASCULAR FSI

### 3.1 Preliminaries

The aim of this section is to review recent numerical techniques for the solution of vascular FSI in hemodynamics, with specific attention to the case of the aorta. Since the aorta is characterized by the largest wall thickness, we mainly focused on numerical methods designed and effective for thick structures. The interested reader may refer, e.g., to [158] and references therein for the case of a membrane structure.

In order to make this discussion concise and easily readable, our choice has focused on some relevant techniques developed in the last years. This choice implies that the reader is familiar with standard numerical issues and terminology concerning FSI for hemodynamics, which are briefly summarized in what follows (for a general overview, see, e.g., [158]):

- *Space discretization for ALE formulation*: The harmonic extension (1f)-(1g) is solved in practice on the computational mesh, so that the update of the fluid domain has to be intended for the mesh points.
  The choice of the ALE formulation is particularly suited when a Finite Element (FE) space discretization is used. Indeed, given the vectorial basis function $\boldsymbol{\phi}_j = \boldsymbol{\phi}_j(\boldsymbol{x}(t))$ in the node $\boldsymbol{x}_j = \boldsymbol{x}_j(t)$[5], the (material) time derivative of a FE function $\boldsymbol{v}_h = \sum_j v_j \boldsymbol{\phi}_j$ reads
  $$\frac{\delta(\boldsymbol{v}_h(t,\boldsymbol{x}))}{\delta t} = \frac{\delta}{\delta t}\left(\sum_j v_j(t)\boldsymbol{\phi}_j(\boldsymbol{x}(t))\right) = \sum_j \frac{dv_j(t)}{dt}\boldsymbol{\phi}_j(\boldsymbol{x}(t)),$$
  where we have exploited that the time variation of the basis functions with respect to the moving fluid domain is zero. This makes the computation of the fluid velocity very easy on the nodes of the fluid mesh; see, e.g., [147].
- *Monolithic solution*: The non-linear system arising from the FSI problem after time discretization (e.g. with a FE approximation) could be solved monolithically through linearization methods, such as Newton or quasi-Newton, and then a suitable monolithic preconditioner is used to efficiently solve the resulting linear system [97];

5. Note that the generic mesh point $\boldsymbol{x}$, and in particular node $\boldsymbol{x}_j$, moves in time according to $\boldsymbol{d}_f$

- *Partitioned strongly-coupled algorithms*: The FSI problem is solved by exploiting separate fluid and structure solvers which exchange the two continuity interface conditions until convergence. In the standard case, the exchange of interface information is based on a Dirichlet condition for the fluid (obtained from the no-slip interface condition (1c)) and a Neumann condition for the structure (obtained from the third Newton interface law (1d)) (*Dirichlet-Neumann* (*DN*) *scheme*). These algorithms are often referred to as *implicit* schemes, since they correspond to the use of implicit time discretizations;
- *Robin interface condition*: To accelerate the convergence of strongly-coupled schemes, Robin interface conditions are built for the fluid and/or structure subproblems as a linear combination of continuity conditions, through the introduction of suitable interface parameters. This leads to the family of *Robin-Robin* (RR) strongly-coupled schemes [14, 11];
- *Partitioned loosely-coupled algorithms*: The FSI problem is solved by exploiting separate fluid and structure solvers which are solved exchanging continuity interface conditions only once per time step. These algorithms are often referred to as *explicit* schemes;
- *Added mass effect*: It happens (or in other words, we say that added mass is relevant) when fluid and structure densities are similar, as it occurs for hemodynamics. The main implication of the added mass effect is in general a slow convergence of strongly-coupled schemes and (absolute) stability issues of loosely-coupled schemes. For example, the explicit DN scheme is unconditionally unstable for relevant added mass [45], whereas the implicit DN scheme requires a small relaxation parameter to converge, often estimated by the Aitken procedure [45, 73, 118];
- *Semi-implicit algorithms*: Only the fluid pressure is strongly-coupled with the structure displacement, whereas the geometric and the kinematic couplings are treated explicitly. This leads in general to *CFL-like* bounds on $\Delta t$ which guarantee stability even for high added mass [68, 17].
  A variant of such methods is provided by strongly coupling both fluid velocity and pressure to the structure quantities, and by treating explicitly the geometric coupling. This strategy has been seen to be accurate and stable in the hemodynamics regime [17, 149].

For the time discretization of (1), a common choice is to discretize the fluid and the vessel wall problems with two schemes of equal order, e.g., BDF2 or Crank-Nicolson for the fluid and the Newmark scheme for the vessel problem [158]. In general, we will write:

$$\frac{\partial \boldsymbol{v}(t^n)}{\partial t} \simeq \frac{\alpha \boldsymbol{v}(t^n)}{\Delta t} + \boldsymbol{f}^n, \qquad \frac{\partial^2 \boldsymbol{v}(t^n)}{\partial t^2} \simeq \frac{\beta \boldsymbol{v}(t^n)}{\Delta t^2} + \boldsymbol{g}^n,$$

for suitable constants $\alpha$ and $\beta$ and functions $\boldsymbol{f}^n$ and $\boldsymbol{g}^n$, and where $t^n = n\Delta t$ for $n = 0, 1, \ldots,$ $\Delta t$ being the time step.

For the sake of simplicity, if not otherwise specified, in the schemes detailed below for the vascular FSI problem, we consider an explicit treatment of the

geometric coupling as well as a semi-implicit treatment of the convective term[6]. In particular, for a generic function or domain $v(t)$, we introduce the approximations $v^n \simeq v(t^n)$ and the extrapolation $v^*$ from previous time steps of the same order of the time discretization.

## 3.2 Strongly-coupled partitioned algorithms

We start with a review of recent improvements in fully coupled schemes. Given the interface parameters $\sigma_f$ and $\sigma_s$, a general scheme is given by the following:
*Implicit Robin-Robin scheme.* For $n \geq 1$, $k \geq 1$, at time step $t^n$/iteration $k$:

**1.** Solve the Oseen problem with a Robin condition at the FS interface:

$$\frac{\rho_f \alpha}{\Delta t}\boldsymbol{u}^n_{(k)} + \rho_f(\boldsymbol{u}^* - \boldsymbol{u}^*_f)\cdot\nabla\boldsymbol{u}^n_{(k)} - \nabla\cdot\boldsymbol{T}_f(\boldsymbol{u}^n_{(k)}, p^n_{(k)}) = \boldsymbol{g}^n_f \qquad \text{in } \Omega^*_f, \tag{2a}$$

$$\nabla\cdot\boldsymbol{u}^n_{(k)} = 0 \qquad \text{in } \Omega^*_f, \tag{2b}$$

$$\sigma_f\boldsymbol{u}^n_{(k)} + \boldsymbol{T}_f\left(\boldsymbol{u}^n_{(k)}, p^n_{(k)}\right)\boldsymbol{n}^* = \sigma_f\left(\frac{\alpha}{\Delta t}\boldsymbol{d}^n_{(k-1)} + \boldsymbol{f}^n\right) + \boldsymbol{T}_s\left(\boldsymbol{d}^n_{(k-1)}\right)\boldsymbol{n}^* \quad \text{on } \Sigma^*; \tag{2c}$$

**2.** Solve the (non-linear) vessel wall problem with a Robin condition at the FS interface:

$$\frac{\rho_s\beta}{\Delta t^2}\widehat{\boldsymbol{d}}^n_{(k)} - \nabla\cdot\widehat{\boldsymbol{T}}_s\left(\widehat{\boldsymbol{d}}^n_{(k)}\right) = \widehat{\boldsymbol{g}_s}^n \qquad \text{in } \widehat{\Omega}_s, \tag{3a}$$

$$\frac{\sigma_s\alpha}{\Delta t}\widehat{\boldsymbol{d}}^n_{(k)} + \widehat{\boldsymbol{T}}_s\left(\widehat{\boldsymbol{d}}^n_{(k)}\right)\widehat{\boldsymbol{n}} = \sigma_s\widehat{\boldsymbol{u}}^n_{(k)} + \widehat{\boldsymbol{T}}_f\left(\widehat{\boldsymbol{u}}^n_{(k)}, \widehat{p}^n_{(k)}\right)\widehat{\boldsymbol{n}} - \sigma_s\widehat{\boldsymbol{f}}^n \quad \text{on } \widehat{\Sigma}; \tag{3b}$$

**3.** If the stopping criterion

$$\sigma_f\left\|\boldsymbol{u}^n_{(k)} - \frac{\alpha}{\Delta t}\left(\boldsymbol{d}^n_{(k)} + \boldsymbol{f}^n\right)\right\|_{H^{1/2}(\Sigma)} + \left\|T_f\left(\boldsymbol{u}^n_{(k)}, p^n_{(k)}\right) - T_s\left(\boldsymbol{d}^n_{(k)}\right)\right\|_{H^{-1/2}(\Sigma)} < \varepsilon$$

is satisfied, then $n \longrightarrow n+1$. Otherwise, $k \longrightarrow k+1$.

In the previous algorithm, $\boldsymbol{n}$ is the outward unit normal to $\Sigma$, $\varepsilon$ a suitable tolerance, and $\boldsymbol{g}^n_f$, $\boldsymbol{g}^n_s$ represent terms coming from time discretization.

A recent analysis has been performed in [58] for the DN scheme ($\sigma_f \longrightarrow \infty$, $\sigma_s = 0$). In particular, the authors proposed to use a relaxation for both the interface conditions: given a single relaxation parameter $\omega$, the fluid problem (2a)-(2b) is equipped with

$$\boldsymbol{u}^n_{(k)} = \frac{\alpha}{\Delta t}\left(\omega d^n_{(k-1)} + (1-\omega)d^n_{(k-2)}\right) + \boldsymbol{f}^n \quad \text{on } \Sigma^*,$$

6. This leads to a bound on $\Delta t$ which is however mild with respect to accuracy requirements [159]

whereas the structure problem (3a) with

$$\widehat{\boldsymbol{T}}_s\left(\widehat{\boldsymbol{d}}^n_{(k)}\right)\widehat{\boldsymbol{n}} = \omega\widehat{\boldsymbol{T}}_f\left(\widehat{\boldsymbol{u}}^n_{(k)}, \widehat{p}^n_{(k)}\right)\widehat{\boldsymbol{n}} + (1-\omega)\widehat{\boldsymbol{T}}_f\left(\widehat{\boldsymbol{u}}^n_{(k-1)}, \widehat{p}^n_{(k-1)}\right)\widehat{\boldsymbol{n}} \quad \text{on } \widehat{\Sigma}.$$

From the analysis of a model problem (2D potential flow coupled with a 1D membrane, see [45]), the authors found the optimal choice

$$\omega_{opt} = \frac{2\sqrt{\xi}}{1+\sqrt{\xi}},$$

for a first order time discretization, where $\xi = \min_k \frac{\rho_s H_s}{\rho_s H_s + \rho_f \mu_i}$, $H_s$ is the structure thickness, and $\rho_f \mu_i$ is the added mass corresponding to frequency $i$ (see [58] for further details). This method provides improvements in the convergence with respect to standard DN iterations, while preserving non-intrusion in available codes.

In [67] the authors showed that, extending the arguments reported in [150] for the membrane case, the monolithic FSI problem is equivalent to an implicit splitting where, at the continuous level, the structure is equipped with the Neumann condition coming from the dynamic continuity condition, whereas on the fluid the following *generalized* Robin condition is imposed:

$$\rho_s \boldsymbol{B}_h \frac{\partial \boldsymbol{u}}{\partial t} + \boldsymbol{T}_f(\boldsymbol{u}, p)\,\boldsymbol{n} = \rho_s \boldsymbol{B}_h \frac{\partial^2 \boldsymbol{d}}{\partial t^2} + \boldsymbol{T}_s(\boldsymbol{d})\,\boldsymbol{n} \qquad \text{on } \Sigma, \tag{4}$$

where $\boldsymbol{B}_h$ is an interface operator built on the lumped-mass inner product, thus diagonal with respect to the interface Finite Element basis. At the discrete level, in particular for a first-order time discretization, this leads to iterations (2)-(3) with

$$\sigma_f = \frac{\rho_s}{\Delta t}\boldsymbol{B}_h \qquad \sigma_s = 0,$$

where $\sigma_f$ should be here thought as an interface operator[7]. The authors proved the convergence of such iterations and showed their suitability for numerical simulations in 3D simplified geometries in the hemodynamic regime. In particular, convergence is improved with respect to other standard choices of the Robin parameters obtained by analyses based on flat interface, see, e.g., [82].

Other recent works tried to optimize the interface parameters $\sigma_f$ and $\sigma_s$ through analyses performed in non-flat scenarios, in order to account for the vascular shape and to improve the convergence of iterations (2)-(3). Starting from the model problem proposed in [45], extended to the case of a cylindrical geometry (see also [200]), in [88] the authors used the Optimized Schwarz Method [77, 86] to find suitable Robin interface parameters. The inclusion of the curvature in the analysis, by means of the cylindrical geometry, made

7. At the algebraic level, the matrix counterpart of $\boldsymbol{B}_h$ is nothing but the diagonal lumped mass matrix referred to the interface degrees of freedom

it possible to account for the specific shape of blood vessels and to improve convergence with respect to 2D/flat analyses[8]. In particular, set

$$A(m,i) = -\frac{\lambda\Delta t\beta\left(K'_m(\beta R) - \chi\, I'_m(\beta R)\right)}{K_m(\beta R) - \chi\, I_m(\beta R)}, \quad B(m,i) = -\frac{\rho_f\, I_m(iR)}{\Delta t\, i\, I'_m(iR)},$$

$$\beta(i) = \sqrt{i^2 + \frac{\rho_s}{\lambda\Delta t^2}}, \quad \chi(m,i) = \frac{K'_m(\beta(R+H))}{I'_m(\beta(R+H))},$$

$$\overline{B} := \max_{(m,i)\in K} B\,(m,i)\,, \quad \overline{A} := \min_{(m,i)\in K} A\,(m,i)\,, \quad \overline{M} = \frac{1}{2}\left(\overline{A} + \overline{B}\right),$$

$$D\,(m,i) = \frac{1}{2}\left(A\,(m,i) - B\,(m,i)\right), \qquad M\,(m,i) = \frac{1}{2}\left(A\,(m,i) + B\,(m,i)\right),$$

$$Q\,(m,i) = \frac{|M\,(m,i) - \overline{M}|}{D\,(m,i)},\ \overline{Q} = \sup_{(m,i)\in K} Q\,(m,i)\,,\ N = \frac{\inf_{(m,i)\in K} D\,(m,i)}{\sup_{(m,i)\in K} D\,(m,i)},$$

$$\rho_0 = \max\left\{\left(\frac{1-\sqrt{N}}{1+\sqrt{N}}\right)^2; \left(\frac{1-\sqrt{1-\overline{Q}^2}}{\overline{Q}}\right)^2\right\},$$

where: $i \geq 0$ and $m = 0, 1, 2, \ldots$ are the frequencies related to the axial and circumferential coordinates, respectively, and which belong to the set $K$, $R$ is the radius of the lumen, $H$ is the structure thickness, $\lambda$ is a surrogate elastic structure parameter, and $I_m$ and $K_m$ are the modified Bessel functions. In particular, optimal choices for interface parameters are of the form

$$\sigma_f = p \qquad \sigma_s = -p + 2\overline{M}, \tag{6}$$

where $p \in [p_-, p_+]$ with

$$p_- = \overline{M} + \sup_{(m,i)}\left\{\frac{1+\rho_0}{1-\rho_0} D\,(m,i) - \sqrt{\left(\overline{M} - M\,(m,i)\right)^2 + \frac{4\rho_0}{(1-\rho_0)^2} D^2\,(m,i)}\right\},$$

$$p_+ = \overline{M} + \inf_{(m,i)}\left\{\frac{1+\rho_0}{1-\rho_0} D\,(m,i) + \sqrt{\left(\overline{M} - M\,(m,i)\right)^2 + \frac{4\rho_0}{(1-\rho_0)^2} D^2\,(m,i)}\right\}.$$

The previous result guarantees fast convergence for any frequencies $(m,i) \in K$. Moreover, this range contains the optimal value which could be easily found numerically. Numerical experiments in real vascular geometries in the hemodynamic regime highlighted that the previous choice made it possible to halve the number of iterations with respect to the Aitken-DN scheme. An

8. The analysis performed in a cylindrical geometry to find optimal interface Robin parameters to be used for real vessels does not introduce any error per se, the solution at convergence of (2)-(3) being "exact" (up to tolerances). However, the greater the deviation from the ideal case, the slower the convergence velocity

extension to the case of spherical geometries with an application to Abdominal Aortic Aneurysms (AAA) has been provided in [87].

The delicate issue of selecting the Robin interface parameters in order to have a good convergence is partially overcome by the *Robin-Neumann/Quasi-Newton scheme* proposed in [174]. For the Neumann condition for the structure ($\sigma_s = 0$), it is proposed to "relax" the fluid traction by mean of an *Interface Quasi-Newton* method, firstly introduced in the context of FSI in [55]. In particular, for a given time instant, at iteration $k$, let $W_k$ be the rectangular matrix whose $k$ columns are the increments of the Finite Element (non-relaxed) fluid traction vectors $\widetilde{\boldsymbol{h}}_{(k)}$ between two consecutive iterations and let $V_k$ be the same built on the discrepancies between two consecutive residuals, where the latter is defined as the difference between the relaxed and non-relaxed tractions: $\boldsymbol{R}_i = \widetilde{\boldsymbol{h}}_{(i)} - \boldsymbol{h}_{(i)}$. Then, the relaxation step reads

$$\boldsymbol{h}_{(k+1)} = \widetilde{\boldsymbol{h}}_{(k)} + W_k \boldsymbol{\alpha}_k \qquad \boldsymbol{\alpha}_k = \text{argmin}_{\boldsymbol{\beta} \in \mathbb{R}^k} \|V_k \boldsymbol{\beta} + \boldsymbol{R}_k\|_2.$$

A more efficient variant is obtained by including information also at previous time steps in $V_k$ and $W_k$. Regarding the latter case, the authors showed 3D numerical results with high added mass effect, highlighting the excellent convergence properties of the method, which are independent of the value of $\sigma_f$ in a wide range of values. A further improvement has been performed in [173], where the authors proposed a way to avoid any explicit Jacobian approximation, so that the multi-vector update is realized with linear complexity.

In [36], the authors proposed an adaptive time step strategy, which works well in case of relevant added mass effect. The idea is to select $\theta \in [0.5, 1]$, introduce the intermediate unknowns, e.g.

$$\boldsymbol{u}_{(0)}^{n+\theta} = (1+\theta)\boldsymbol{u}^n - \theta \boldsymbol{u}^{n-1},$$

a similar expression for $\boldsymbol{d}$, and

$$p_{(0)}^{n+\theta} = (1+\Delta t^n) p^{n-1+\theta} - \Delta t^{n-1} p^{n-2+\theta},$$

and then solve iterations (2)-(3) with a first-order time discretization for $\boldsymbol{u}^{n+\theta}$, $p^{n+\theta}$, $\boldsymbol{d}^{n+\theta}$ until convergence with the case $\alpha_f = \alpha_s$ suitably chosen. Then, with such solutions, perform an explicit step:

$$\boldsymbol{u}^{n+1} = \frac{1}{\theta}\boldsymbol{u}^{n+\theta} - \frac{1-\theta}{\theta}\boldsymbol{u}^n$$

(a similar expression for $\boldsymbol{d}$ holds true), and compute the new time step

$$\Delta t^{n+1} = \Delta t^n \min\left\{ r_1, \max\left\{ r_2, s\left( \frac{\delta}{\|T^{n+1}\|} \right)^{1/3} \right\} \right\},$$

where $r_1, r_2, \delta, s$ are chosen parameters and $T^{n+1}$ is the local truncation error (see [36] for its estimation), and set $t^{n+2} = t^{n+1} + \theta \Delta t^{n+1}$. If $\|T^{n+1}\| \geq \delta$ repeat

time step $n$ with the new time step. Numerical experiments in the hemodynamic regime showed that this method is accurate with respect to the case of fixed (small) $\Delta t$, allowing a significant saving in the computational effort.

### 3.3 Semi-implicit partitioned algorithms

In the framework of semi-implicit algorithms, a quite recent development has been provided in [11], where the use of Robin interface conditions has been proposed as follows:
For $n \geq 1$, at time step $t^n$:

**1.** Solve the pressure-structure coupling: At iteration $k \geq 1$ until convergence

- Solve the (non-viscous) fluid problem with a Dirichlet condition at the FS interface:

$$\begin{aligned}
&\frac{\rho_f \alpha}{\Delta t}\left(\boldsymbol{u}^n_{(k)} - \widetilde{\boldsymbol{u}}^n\right) + \nabla p^n_{(k)} = \boldsymbol{0} && \text{in } \Omega^*_f,\\
&\nabla \cdot \boldsymbol{u}^n_{(k)} = 0 && \text{in } \Omega^*_f,\\
&\boldsymbol{u}^n_{(k)} = \frac{\alpha}{\Delta t}\boldsymbol{d}^n_{(k-1)} + \boldsymbol{f}^n && \text{on } \Sigma^*;
\end{aligned}$$

- Solve the (non-linear) vessel wall problem with a Robin condition at the FS interface:

$$\begin{aligned}
&\frac{\rho_s \beta}{\Delta t^2}\widehat{\boldsymbol{d}}^n_{(k)} - \nabla \cdot \widehat{\boldsymbol{T}}_s\left(\widehat{\boldsymbol{d}}^n_{(k)}\right) = \widehat{\boldsymbol{g}}^n_s && \text{in } \widehat{\Omega}_s,\\
&\frac{\gamma\mu}{h}\frac{\alpha}{\Delta t}\widehat{\boldsymbol{d}}^n_{(k)} + \widehat{\boldsymbol{T}}_s\left(\widehat{\boldsymbol{d}}^n_{(k)}\right)\widehat{\boldsymbol{n}} = \frac{\gamma\mu}{h}\widehat{\boldsymbol{u}}^n_{(k)} + \widehat{\boldsymbol{T}}_f\left(\widehat{\boldsymbol{u}}^n_{(k)}, \widehat{p}^n_{(k)}\right)\widehat{\boldsymbol{n}} - \frac{\gamma\mu}{h}\widehat{\boldsymbol{f}}^n && \text{on } \widehat{\Sigma},
\end{aligned}$$

**2.** Solve the explicit viscous-structure coupling:

$$\begin{aligned}
&\frac{\rho_f \alpha}{\Delta t}\widetilde{\boldsymbol{u}}^n + \rho_f(\widetilde{\boldsymbol{u}}^* - \boldsymbol{u}^*_f)\cdot\nabla\widetilde{\boldsymbol{u}}^n - \nabla\cdot\left(\nabla\widetilde{\boldsymbol{u}}^n + \left(\nabla\widetilde{\boldsymbol{u}^n}\right)^T\right) = \boldsymbol{g}^n_f && \text{in } \Omega^*_f,\\
&\nabla\cdot\widetilde{\boldsymbol{u}}^n = 0 && \text{in } \Omega^*_f,\\
&\frac{\gamma\mu}{h}\widetilde{\boldsymbol{u}}^n + \left(\nabla\widetilde{\boldsymbol{u}}^n + \left(\nabla\widetilde{\boldsymbol{u}}^n\right)^T\right)\boldsymbol{n}^* = \frac{\gamma\mu}{h}\left(\frac{\alpha}{\Delta t}\boldsymbol{d}^n + \boldsymbol{f}^n\right) + \left(\nabla\widetilde{\boldsymbol{u}}^{n-1} + \left(\nabla\widetilde{\boldsymbol{u}}^{n-1}\right)^T\right)\boldsymbol{n}^* && \text{on } \Sigma^*,
\end{aligned}$$

where $\gamma$ is a stabilization parameter and $h$ the mesh size. Notice the use of Robin interface conditions for the structure and the viscous problems, with $\sigma_f = \sigma_s = \frac{\gamma\mu}{h}$. This choice comes from a Discontinuous Galerkin (DG) approach used to "glue" the solutions at the interface (see Section 3.4).

The authors showed that, for a model problem with a first-order time discretization, the previous algorithm is absolutely stable provided that

$$\gamma > 2\,C_t \qquad \gamma\mu\Delta t = O(h),$$

where $C_t$ is the constant of the standard discrete trace-inverse inequality. We observe that, unlike the standard DN-based semi-implicit schemes, the stability

conditions do not depend on the fluid-solid density ratio. Numerical experiments confirmed that the method is robust with respect to the added mass effect and it is able to handle meshes which are non-conforming at the interface.

### 3.4 Loosely-coupled algorithms

One the most important achievement made in the last years in the field of the numerical solution of the FSI problem in the hemodynamic regime is given by the design of stable loosely-coupled schemes. For the sake of brevity and due to the aims of this book, we focus here only on those methods, designed for a thick structure, which were tested in 3D numerical experiments.

In general, the idea of a loosely-coupled scheme could be thought as performing just one iteration over $k$ in (2)-(3), where the two interface conditions become:

$$\begin{aligned} &(F) \quad \sigma_f \boldsymbol{u}^n + \boldsymbol{T}_f\left(\boldsymbol{u}^n, p^n\right)\boldsymbol{n}^* = \sigma_f\left(\frac{\alpha}{\Delta t}\boldsymbol{d}^* + \boldsymbol{f}^*\right) + \boldsymbol{T}_s\left(\boldsymbol{d}^*\right)\boldsymbol{n}^* \quad \text{on } \Sigma^*; \\ &(S) \quad \frac{\sigma_s \alpha}{\Delta t}\widehat{\boldsymbol{d}}^n + \widehat{\boldsymbol{T}}_s\left(\widehat{\boldsymbol{d}}^n\right)\widehat{\boldsymbol{n}} = \sigma_s \widehat{\boldsymbol{u}}^n + \widehat{\boldsymbol{T}}_f\left(\widehat{\boldsymbol{u}}^n, \widehat{p}^n\right)\widehat{\boldsymbol{n}} - \sigma_s \widehat{\boldsymbol{f}}^n \quad \text{on } \widehat{\Sigma}, \end{aligned} \tag{10}$$

where we point out the use of the extrapolation $\boldsymbol{d}^*$ in the fluid interface condition[9].

One of the first loosely-coupled schemes for hemodynamics has been proposed in [41], where a *Nitsche* method based on a DG mortaring has been used to handle the continuity interface conditions. Given the stabilization parameter $\gamma$ and denoting by $h$ the characteristic mesh size, the method, proposed in weak form, corresponds to (10) with $\sigma_s = \frac{\gamma\mu}{h}$ and $\sigma_f = +\infty$ (i.e. a Dirichlet condition for the fluid), where however the fluid condition is treated by means of the Nitsche method. The authors proved that, with this strategy, spurious oscillations of the fluid pressure at the interface arise. To overcome this limitation, they proposed to add a stabilization term for the fluid problem, which in weak form reads

$$\frac{\gamma_0 h}{\gamma\mu}\int_\Sigma \left(p_h^n - p_h^{n-1}\right) q_h,$$

$q_h$ being the pressure test functions. It has been shown that, for a first-order time discretization, stability is now achieved, provided that

$$\gamma \geq 256\, C_t \qquad \gamma\Delta t \leq Ch \qquad \gamma_0 \geq 8.$$

Also, the authors proved that by performing a correction step, corresponding to two strongly-coupled iterations instead of one, a global first order in time is recovered.

Another proposal was derived in [67] where, starting from the identity (4), the authors proposed, for a first-order time discretization, iterations (10) with the

9. The order of the two subproblems could be exchanged, using extrapolated variables $\boldsymbol{u}^*$, $p^*$ for the structure interface condition

choice

$$\sigma_f = \frac{\rho_s}{\Delta t}\boldsymbol{B}_h \qquad \sigma_s = 0,$$

and $\boldsymbol{d}^* = 2\boldsymbol{d}^{n-1} - \boldsymbol{d}^{n-2}$. The authors proved unconditional stability of this method, which is also independent of the added mass, confirmed by some numerical results in 3D simplified geometries. Works on this topic can also be found in [40, 39].

Another recent work that used values of the interface Robin parameters proposed for the strongly-coupled case is reported in [89]. Here the authors used the optimized values (6) as reasonable values to achieve stable results in the case of the loosely-coupled case for arterial vessels. This idea followed from the stability results of the loosely-coupled Robin-Neumann (RN) scheme obtained in [90] for the model problem proposed in [45]. In particular, the authors found that the loosely-coupled RN scheme is:
- unstable if the added mass effect is relevant and $\sigma_f$ is large enough ($\sigma_f > \bar{\sigma}$, with $\bar{\sigma}$ decreasing for increasing added mass);
- stable if $\Delta t$ is small enough ($\Delta t < \bar{\Delta}\, h$, with $\bar{\Delta}$ decreasing for increasing values of $\sigma_f$ and increasing added mass effect).
3D numerical experiments obtained in [89] in an abdominal aorta in presence of an aneurysm showed the reliability of this proposal.

We also mention other loosely-coupled algorithms given by an operator splitting procedure, where the fluid problem is equipped with a part of the structure one [35, 168], as well as the method and analysis provided in [170].

## 3.5 Monolithic strategies

We start by reviewing a class of works that considered a membrane assumption for the structure. Despite the significant thickness of the aortic vessel wall, this assumption could be reasonable when the attention is on blood dynamics. In this case, a smart way to write the monolithic system is to embed the structure membrane problem into the fluid as a proper (in general non-local) boundary condition, see [70] where the authors successfully applied this idea to the aorta. Under the assumption of no shear stresses acting on the membrane, in [150] a monolithic formulation has been derived consisting in the fluid problem equipped by the following boundary condition for the normal component at the interface (for the sake of simplicity, reported under the assumption of fixed fluid domain and no prestress):

$$\left(\frac{\rho_s H_s}{\Delta t} + \beta\Delta t\right) u_\perp^n + \boldsymbol{T}_f\left(\boldsymbol{u}^n, p^n\right)\boldsymbol{n}\cdot\boldsymbol{n} = \left(\frac{\rho_s H_s}{\Delta t} + \beta\Delta t\right) d_\perp^n - \frac{\rho_s H_s}{\Delta t} d_\perp^{n-1} \quad \text{on } \Sigma,$$

where $u_\perp^n$ and $d_\perp^n$ are the normal fluid velocity and structure displacement, and $\beta$ is a coefficient that includes the structure information, i.e.:

$$\beta = \frac{H_s E}{1-\nu^2}\left(4\rho_1^2 - 2(1-\nu)\rho_2\right),$$

where $\nu$ is the Poisson ratio, $E$ the Young modulus, $\rho_1 = \rho_1(t, \boldsymbol{x})$ is the mean curvature at point $\boldsymbol{x}$ of the membrane and $\rho_2 = \rho_2(t, \boldsymbol{x})$ the Gaussian curvature. This approach has been applied to aortic simulations in [51], where a comparison with a full 3D-3D FSI model showed discrepancies of the displacements below 8% and comparable Wall Shear Stresses (WSS) when the same treatment of the geometric coupling is used.

Coming back to the case of a thick structure, in general, monolithic procedures are based on building the non-linear system of equations $\boldsymbol{F}(\boldsymbol{x}) = \boldsymbol{0}$ arising from space discretization (e.g. the Finite Element method) of the FSI problem, including the geometric coupling. Then, the Newton method is applied:

$$J(\boldsymbol{x}_{(k)})\delta\boldsymbol{x}_{(k)} = -\boldsymbol{F}(\boldsymbol{x}_{(k)}) \qquad \boldsymbol{x}_{(k+1)} = \boldsymbol{x}_{(k)} + \delta\boldsymbol{x}_{(k)}. \tag{11}$$

Here $\boldsymbol{x}$ collects the fluid, structure and fluid mesh unknowns, whereas $J$ is the Jacobian matrix. A well-established strategy consists in introducing a block preconditioner for the linearized FSI system (11), exploiting the separate solution of the three subproblems (fluid, structure, fluid geometry) [97].

In this respect, a recent method to efficiently solve the previous Newton iteration has been proposed in [56], where the authors introduce a Lagrange multiplier $\boldsymbol{\lambda}$ to enforce the no-slip interface condition and then solve (11) (adapted to the case of this further unknown and reordering the unknowns as follows: $\boldsymbol{d}$, $\boldsymbol{d}_f$, $(\boldsymbol{u}_f, p)$, $\boldsymbol{\lambda}$) with a right-preconditioned GMRES, where the block preconditioner for $J(\boldsymbol{x}_{(k)})$ is built by:

- neglecting the Lagrange multiplier block $-I_\Sigma^T$ in the structure equation (i.e. the term in position 1,4):

$$\begin{pmatrix} S & 0 & 0 & 0 \\ -I_\Sigma & G & 0 & 0 \\ 0 & D & F & I_\Sigma^T \\ -\frac{\zeta}{\Delta t} I_\Sigma & 0 & I_\Sigma & 0 \end{pmatrix},$$

  where $S, G, F$ are the linearized structure, geometry and fluid problems, $D$ the shape derivatives, coming from the derivative of the fluid problem with respect to the fluid mesh displacement, and $\zeta$ accounts for the time discretization of $\frac{\partial \boldsymbol{d}}{\partial t}$ in the no-slip condition (fourth row);
- approximating $S$ and $G$ by suitable ad-hoc preconditioners (e.g. 1-level algebraic additive Schwarz preconditioners);
- eliminating from the fluid problem row the unknowns of the fluid interface velocity and of the Lagrange multiplier, by static condensation;
- applying the SIMPLE preconditioner [61] for the resulting fluid problem.

Numerical results in realistic 3D hemodynamic problems of this algorithm showed scalability up to thousands of cores with about 150 millions of degrees of freedom, featuring also robustness with respect to mesh size.

A variant of this method has been proposed in [80], where the interface variables are removed directly from the set of unknowns of the FSI problem

and not at the preconditioner level, multigrid solvers are used for the three subproblems, and the boundary condition at $\Sigma$ for the fluid and structure problems are inverted (Dirichlet for the structure and Neumann for the fluid). The major drawback of this approach is that the coupling is realized only on the finest meshes of multigrid algorithms. To overcome this limitation, in [80] the authors proposed to switch the role of multigrid approach and preconditioner, using the former approach in a global sense directly to (11) and the latter as smoothing. This method was successfully applied to a realistic case of AAA.

*Inexact-Newton* strategies were often preferred to the Newton one, despite the loss of second-order convergence, since the increase in the number of iterations is well compensated by the simplification in the construction of the approximate Jacobian $\widetilde{J}_k$. In this respect, a *Domain Decomposition*-based approach has been proposed in [198], where the authors introduced a "right preconditioner":

$$\widetilde{J}_k = J(\boldsymbol{x}_{(k)})M_k^{-1}M_k,$$

with $M_k^{-1}$ being a restricted additive Schwarz preconditioner, to be solved with GMRES. The partition of the mesh in overlapped subdomains is completely independent of the physical variables, so that a subdomain may contain both fluid and structure elements. In particular, the preconditioned residual $M_{(k)}^{-1}\boldsymbol{r}$ at each GMRES iteration is computed as follows:

$$B_\ell z_\ell = R_\ell \boldsymbol{r} \qquad M_k^{-1}\boldsymbol{r} = \sum_{\ell=1}^{N} \left(R_\ell^0\right)^T z_\ell, \tag{12}$$

where $N$ is the number of subdomains, $B_\ell = R_\ell J(\boldsymbol{x}_{(k)})R_\ell^T$, with $R_\ell$ mapping the global vector of unknowns to those belonging to the $\ell$-th overlapping subdomain, and $R_\ell^0$ is the restriction of the degrees of freedom to the non-overlapped counterpart of the $\ell$-th subdomain. The linear systems in (12) are solved with an ILU factorization procedure. 3D numerical results showed the strong scalability of the method even for realistic vascular geometries and with about ten million unknowns.

Another type of inexact-Newton method for FSI has been introduced, where the Jacobian matrix is obtained by neglecting the shape derivatives [180]. This approach reduces the complexity of assembling the Jacobian matrix by preventing the solution of extra differential problems to compute the shape derivatives entries. This simplification has been shown to be robust in terms of convergence of the Newton loop, allowing to obtain efficient and significant results for realistic aortic simulations, see [52, 148]. In the latter work, a strategy based on two nested loops was also proposed: the external one (inexact-Newton) to manage the geometric coupling and the inner one to handle the kinematic and dynamic conditions, e.g., by means of a Robin-Robin preconditioner. In this respect, it is enough to set the tolerance of the RR iterations proportional to the external inexact-Newton residual without affecting the accuracy [113]. This ap-

proximately halves the number of RR iterations (e.g. passing from, on average, 7.7 to 3.0 iterations for the case of the aorta).

## 3.6 Methods based on the interface equation

From the Domain Decomposition (DD) theory, it is known that the algebraic interface equation (e.g. coming from the Finite Element discretization after application of the Newton method), corresponding to a block Gaussian elimination of the internal unknowns, is better conditioned than the monolithic system. Starting from this, in [69] the interface equation

$$S_s^{-1}\left(S_f(\boldsymbol{\lambda})\right) - \boldsymbol{\lambda} = 0,$$

corresponding to the FSI monolithic problem has been derived and successfully solved with the Newton method in 3D blood flow simulations. Here, $S_f$ and $S_s$ represent the non-linear maps that, taken an interface displacement $\boldsymbol{\lambda}$, return the interface traction associated to the fluid problem (together with the fluid geometric one) and the structure problem, respectively.

Starting from this, in [57] the authors studied different standard DD preconditioners (adapted to the non-linear case) and verified their suitability to solve realistic 3D hemodynamic problems. This was done by considering the preconditioned Richardson method over the Steklov-Poincaré (Schur complement at the algebraic level) equation:

$$P\left(\boldsymbol{\lambda}^{(k+1)} - \boldsymbol{\lambda}^{(k)}\right) = \omega^k\left(-S_f\left(\boldsymbol{\lambda}^{(k)}\right) - S_s\left(\boldsymbol{\lambda}^{(k)}\right)\right),$$

with $\omega^k$ an acceleration parameter and $P$ the preconditioner, i.e.'$S_s'(\boldsymbol{\lambda}^{(k)})$ (Dirichlet-Neumann preconditioner) and $\left(\alpha_f^k S_f'(\boldsymbol{\lambda}^{(k)})^{-1} + \alpha_s^k S_s'(\boldsymbol{\lambda}^{(k)})^{-1}\right)^{-1}$ (with $\alpha_f^k + \alpha_s^k = 1$, Neumann-Neumann preconditioner), and where by $'$ we indicate the tangent problem.

An improvement in this direction has been performed in [16] where the authors proposed to use the DN preconditioner in combination with GMRES instead of Richardson to solve the Schur complement equation. Test on realistic 3D hemodynamic problems showed that this method allowed to improve convergence but not to overcome the limitations due to the added mass effect. This has been solved in [15] where a Robin-Robin interface preconditioner

$$P_{RR} = \frac{1}{\sigma_f + \sigma_s}\left(S_f'(\boldsymbol{\lambda}^{(k)}) + \sigma_f I_\Sigma\right) I_\Sigma^{-1}\left(S_s'(\boldsymbol{\lambda}^{(k)}) + \sigma_s I_\Sigma\right)$$

has been used with GMRES for the Schur complement interface equation, $I_\Sigma$ being the identity operator at the interface (or, equivalently, the interface mass matrix for the Finite Element method). Numerical results for 3D blood flow problems revealed very good convergence properties, which are quite independent of the added mass and on the choice of $\sigma_f, \sigma_s$.

## 4 NUMERICAL APPROACHES FOR AORTIC VALVE FSI

In the case of FSI model arising between blood flow and Aortic Valve (AV), a different perspective is in general needed with respect to the vascular case, since:
- the structure is now immersed in the fluid and
- the structure displacement reaches up to 100% of its dimension.

A broad spectrum of numerical methods has been proposed in the literature for this problem, from the ALE method to several body-fitted and unfitted methods. This section aims at reviewing those of such methods that have most recently been developed or applied to the AV. More general reviews on valve modeling, considering also other cardiac valves, can be found, e.g., in [191, 137, 1].

To simplify the discussion, in this section we neglect the motion of the aortic wall, and we consider the AV as the only structure moving and interacting with the blood flow. The generalization to the case of concurring vascular FSI and valve FSI adds up to a combination of methods presented in different sections. Examples can be found in the very same references that we will present in this section.

Since the focus of this book is on FSI, we also point out that no structure-structure interaction will be discussed, being it either the (self-)contact between different structures or the insertion of the valve leaflets into the aortic annulus. The interested reader may refer to, e.g., [13, 140, 136, 138, 31, 103, 98, 197].

### 4.1 Preliminaries

As mentioned in Section 1, the valve leaflets undergo very large displacement, and their opening and closing induces topological changes in the fluid domain $\Omega_f^t$. For this reason, a wide range of mathematical models and numerical methods have been introduced and employed for valve modeling. Moreover, most models were born to address specific issues raised by the Finite Element discretization of the valve FSI problem, therefore they are strongly connected with the numerical method employed to solve the equations. Different kinds of classifications can be used to categorize these models: in this section, we combine different perspectives to systematize the description, and we adopt the following naming conventions.

- 2*D vs.* 3*D valve modeling*: Aortic valve leaflets are much thinner than the aortic wall, having a typical physiological thickness of less than a millimeter [164, 91]. Therefore, many valve FSI models consider the valve as a 2D surface $\Sigma_v$ moving in the bloodpool, with a dynamics that is described by shell, membrane or other surface elasticity models [197, 124, 183, 107]. These models have proven to be accurate and efficient in representing the valve dynamics and also the effects of valve tissue fibers or calcifications [115, 195]. However, when a very detailed geometrical description of the leaflets is required, and the cross-thickness heterogeneity of physical properties and internal stresses is of interest, a 3D mechanical description of the valve is

needed: the valve occupies a region $\Omega_v$ and the actual fluid-structure interface is its boundary $\partial\Omega_v$. The numerical simulation of these models typically requires a high computational cost, due to the high mesh fineness required to accurately capture the dynamics of the thin leaflets.

- *Body-fitted mesh, unfitted mesh, and Cut Finite Element methods*:
  In methods with a *body-fitted* mesh, the mesh is conforming to the fluid-valve interface, as in the case of ALE methods [119, 144, 112, 194] and the Space-Time Finite Element method [104, 179, 178, 99]. These methods are very accurate in capturing the interface velocity and exchanged stresses, but their application to cardiac valves entails a large distortion of the mesh elements and typically a frequent remeshing. Because of that, they are very difficult to employ in clinical applications, and we refer the reader to [191, 137, 1] for their discussion.
  *Unfitted*-mesh methods have a completely different approach: the fluid mesh is fixed, the moving structure mesh is completely independent, and the interaction between the two is modeled by a modification of the momentum equations, with the introduction of additional terms. This is the case of the *Immersed Boundary* (IB) and *Fictitious Domain* (FD) methods, discussed in Section 4.2, and the *Resistive* and other kinematic methods of Section 4.3.
  A somehow in-between approach is that of *Cut Finite Element* (CFE) methods. Again, the fluid mesh is fixed and a separate moving mesh is considered for the structure. However, instead of modifying the momentum equations, the interface conditions are imposed directly at the intersection between the two meshes, thanks to proper cutting and integration over the elements crossed by the interface. Different methods pertain to the CFE class, and they are going to be reviewed in Section 4.4.

It is worth to point out that the separation between body-fitted, unfitted, and CFE methods above is not airtight: variants and hybrid methods have been proposed in the literature, such as the fixed-mesh ALE approach [50, 208] or the hybrid immersed-boundary/body-fitted-grid method [192].

We notice that CFE methods seem promising for the accurate treatment of both surface and bulk structures, however nowadays their applications to FSI in the hemodynamic regime are almost all still in 2D geometries (see [185] for an idealized 3D AV case). Therefore, their use in realistic AV modeling is not yet as mature as it is for the consolidated IB/FD methods and (to a lesser extent) for the relatively recent resistive approach.

## 4.2 An update on Immersed Boundary & Fictitious Domain strategies

A large portion of the fixed-mesh methods for the modeling of cardiac valves belongs to the classes of IB and FD methods. In the present section, we focus on recent advancements in such methods aimed at the application to AV modeling.

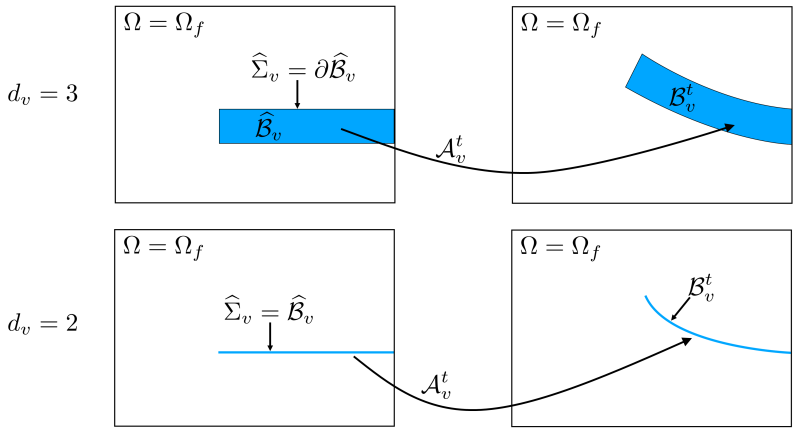


**FIGURE 3** Domain for valve FSI with the IB and FD methods, in the case $\Omega \equiv \Omega_f$: reference (left) and current (right) configuration of the valve modeled as a bulk body (above) or a surface (below).

For a broader discussion of these methods, encompassing also other types of applications, we refer the reader to [141, 172, 116, 186].

The IB and FD classes are strictly intertwined, and several hybrid strategies have been adopted, making sometimes difficult to distinguish between the two. In this review we adopt the most accepted perspective, shared, e.g., by [95, 28, 185]: in IB methods, the fluid momentum equation is modified with the addition of a forcing term related to the residual of the structure problem, while FD methods keep separate formulations for the fluid and solid problem and then couple them by Lagrange multipliers [10].

To set up a common framework for the discussion of different approaches, we introduce some notation, depicted in Fig. 3. In general, we use the same structure quantities of previous sections, with the subscript $v$ instead of $s$. Since both 2D and 3D valve modeling are employed in different works, we denote by $\widehat{\mathcal{B}}_v \subset \mathbb{R}^{d_v}$ (with $d_v = 2, 3$) the valve reference domain, that can either represent a surface $\widehat{\Sigma}_v$ for $d_v = 2$ or a bulk region $\widehat{\Omega}_v$ for $d_v = 3$. The corresponding current configuration is $\mathcal{B}_v^t$, that is the image of the map $\mathcal{A}_v^t : \widehat{\mathcal{B}}_v \to \mathbb{R}^{d_v}$ encoding the positions $\mathcal{A}_v^t(\widehat{\boldsymbol{x}}) = \widehat{\boldsymbol{x}} + \widehat{\boldsymbol{d}}(t, \widehat{\boldsymbol{x}}) \in \mathcal{B}_v^t$ of the structure particles $\widehat{\boldsymbol{x}} \in \widehat{\mathcal{B}}_v$ at each time $t$. With slight abuse of notation, we extend $\mathcal{A}_v^t$ to $\overline{\widehat{\mathcal{B}}_v}$ where needed, so that it is defined also on $\partial\widehat{\mathcal{B}}_v$. The current configurations $\Omega_f$ [11],$\mathcal{B}_v^t$ of the fluid and the valve are both subsets of a background domain $\Omega$ (possibly larger than

10.In several works considering the case of thick structures, Distributed Lagrange Multipliers (DLM) were employed, and the corresponding FD methods are sometimes called DLM methods [95, 28]

11.We remind the reader that in this valve FSI section, $\Omega_f$ is considered as fixed. However, the whole discussion can be easily extended to a moving domain $\Omega_f^t$

$\overline{\Omega_f} \cup \overline{\mathcal{B}_v^t}$). A single Eulerian velocity field $\boldsymbol{u}$ is defined over the whole domain $\Omega$, representing both the fluid and the solid velocity. Moreover, for the sake of exposition, we assume $\nabla \cdot \boldsymbol{u} = 0$ to hold in the whole $\Omega$, that is that also the valve tissue is incompressible. This is a very common assumption in IB methods for the aortic valve and more in general in the valve modeling literature.

In these settings, the FSI system corresponding to a general IB method reads as follows [12]:

$$\rho_f \left( \frac{\partial \boldsymbol{u}}{\partial t} + \boldsymbol{u} \cdot \nabla \boldsymbol{u} \right) - \nabla \cdot \boldsymbol{T}_f(\boldsymbol{u}, p) = \boldsymbol{F} + \boldsymbol{F}_\partial \qquad \text{in } \Omega, \tag{13a}$$

$$\nabla \cdot \boldsymbol{u} = 0 \qquad \text{in } \Omega, \tag{13b}$$

$$\int_\Omega \boldsymbol{u}(t, \boldsymbol{x}) \delta(\boldsymbol{x} - \mathcal{A}_v^t(\widehat{\boldsymbol{x}}))\, d\boldsymbol{x} = \frac{\partial \widehat{\boldsymbol{d}}}{\partial t}(t, \widehat{\boldsymbol{x}}) \qquad \text{for } \widehat{\boldsymbol{x}} \in \widehat{\mathcal{B}}_v, \tag{13c}$$

$$\boldsymbol{F}(t, \boldsymbol{x}) = \int_{\widehat{\mathcal{B}}_v} f_v(t, \widehat{\boldsymbol{x}}) \delta(\boldsymbol{x} - \mathcal{A}_v^t(\widehat{\boldsymbol{x}}))\, d\widehat{\boldsymbol{x}} \qquad \text{for } \boldsymbol{x} \in \Omega, \tag{13d}$$

$$\boldsymbol{F}_\partial(t, \boldsymbol{x}) = \int_{\partial \widehat{\mathcal{B}}_v} f_{v,\partial}(t, \widehat{\boldsymbol{x}}) \delta(\boldsymbol{x} - \mathcal{A}_v^t(\widehat{\boldsymbol{x}}))\, d\widehat{\boldsymbol{x}} \qquad \text{for } \boldsymbol{x} \in \Omega, \tag{13e}$$

where $f_v, f_{v,\partial}$ are suitable force densities, modeling the dynamics of the valve and its boundary, and thus taking different expressions according to the specific IB method of choice. Equation (13c) corresponds to the kinematic condition (1c) presented for vascular FSI, while (13d)-(13e) encode at the same time the structure problem (1e) and the dynamic condition (1d). We notice from (13a) that the momentum equation of the fluid problem is extended from $\Omega_f$ to the background domain $\Omega$: indeed, in the IB framework the fluid and the structure "coexist" in each point of $\Omega$.

The original IB method was introduced in [154] for valve modeling in the Finite Differences framework. In the same framework, it has been enhanced and employed in several FSI studies of the AV, both in the case of bulk ($d_v = 3$) [129, 125] and surface ($d_v = 2$) [94, 93, 188, 169, 204] valves, and the structuredness of a Cartesian background mesh has been exploited for GPU-based parallelization [189]. More recent developments of this method have been introduced to address some of the drawbacks of the Finite Difference IB formulation, such as possibly poor conservation properties, a difficult reconstruction of a suitable approximated $\delta$ function, strong fineness requirements on the structure mesh [26], and the difficulty of managing non-uniform meshes. However, so far, most of these

12. The convolution with the Dirac measure $\delta(\boldsymbol{x} - \mathcal{A}_v^t(\widehat{\boldsymbol{x}}))$ corresponds to the composition with the map $\mathcal{A}_v^t$: for any functions $g_1 : \Omega \to \mathbb{R}$, $g_2 : \widehat{\mathcal{B}}_v \to \mathbb{R}$, it holds:

$$\int_\Omega g_1(\boldsymbol{x})\, \delta(\boldsymbol{x} - \mathcal{A}_v^t(\widehat{\boldsymbol{x}}))\, d\boldsymbol{x} = g_1(\mathcal{A}_v^t(\widehat{\boldsymbol{x}})),$$
$$\int_{\widehat{\mathcal{B}}_v} g_2(\widehat{\boldsymbol{x}})\, \delta(\boldsymbol{x} - \mathcal{A}_v^t(\widehat{\boldsymbol{x}}))\, d\widehat{\boldsymbol{x}} = g_2((\mathcal{A}_v^t)^{-1}(\boldsymbol{x}))$$

enhanced methods have been either employed on simplified geometries or applied to other fields than cardiac valve modeling. For example, an $L^2$-projection operator between the fluid and solid grid was proposed in [145] to improve mass conservation, and tested on benchmark FSI problems, while [193] use the Reproducing Kernel Particle Method (RKPM) to approximate the $\delta$ function and enforce the FSI coupling conditions [13].

To address the issue of geometric accuracy on a fixed grid, the Curvilinear Immersed Boundary (CURVIB) method has been introduced in [78, 32]. The method employs a curvilinear description of the immersed surface, and it has been applied to the simulation of prosthetic valves [121, 10].

The extension of the IB method to Finite Element schemes, introduced in [25, 26, 27], provides a more flexible framework to account simultaneously for immersed surfaces and thick structures. Its variational formulation allows to treat the Dirac $\delta$ directly, possibly without the need for a smooth approximation. Moreover, it naturally allows a quantification of the possible non-conservation errors introduced by the numerical discretization. In these settings, the force density $f_v$ modeling the valve dynamics is related to the residual of the structure problem, namely [14]

$$f_v = -(\rho_v - \rho_f)\frac{\partial^2 \widehat{\boldsymbol{d}}}{\partial t^2} + \nabla \cdot \widehat{\boldsymbol{T}}_v \qquad \text{in } \widehat{\mathcal{B}}_v, \tag{14}$$

while the boundary force density $f_{v,\partial}$ models the transmission force:

$$f_{v,\partial} = -\widehat{\boldsymbol{T}}_v \boldsymbol{n} \qquad \text{on } \partial\widehat{\mathcal{B}}_v. \tag{15}$$

In definition (14), we highlight that the difference $\rho_v - \rho_f$ of the densities appears in the inertial term: this represents a correction to remove the artificial effect of considering the fluid to be coexisting with the solid in $\mathcal{B}_v^t$. In many cases, the densities of the valve and the blood are assumed to be equal, therefore (14) reduces to $f_v = \nabla \cdot \widehat{\boldsymbol{T}}_v$.

A similar IB method, combining the variational Finite Element setting with the RKPM for the enforcement of the interface conditions, was introduced in [202, 201].

We now introduce a general formulation for the FD methods, using the same notation as for the IB methods. A significant difference is that, instead of considering the fluid and the valve to be coexisting in $\mathcal{B}_v^t$, we consider the two

13.We deem all the works mentioned in this paragraph as pertaining to the Finite Differences framework, although a Finite Element discretization of the sole structure problem is sometimes considered. Indeed, all of them rely on a Finite Difference scheme for the fluid problem and (most importantly for the purpose of this review) for the enforcement of the FSI coupling conditions

14.As mentioned in Section 4.1, in the case of surface modeling of the valve, shell, membrane or other mechanical models are considered: up to a consistent modification of the definitions (14)-(15) of the force densities, the whole present discussion still holds

phases separately:

$$\boldsymbol{u} = \begin{cases} \boldsymbol{u}_f & \text{in } \Omega \setminus \mathcal{B}_v^t, \\ \boldsymbol{u}_v & \text{in } \mathcal{B}_v^t, \end{cases} \qquad p = \begin{cases} p_f & \text{in } \Omega \setminus \mathcal{B}_v^t, \\ p_v & \text{in } \mathcal{B}_v^t. \end{cases}$$

The general formulation of FD methods can be naturally represented in weak form, with suitable definitions of test and trial spaces that may depend on the dimension $d_v$ and on the specific method of choice. We refer the reader to [28, 13] for examples of rigorous mathematical formulations. For simplicity, we denote by $V, Q, \widehat{W}$ the spaces for $\boldsymbol{u}, p, \widehat{\boldsymbol{d}}_v$, being $V, Q$ subspaces of $H^1(\Omega), L^2(\Omega)$ and $\widehat{W}$ a subspace of $H^1(\widehat{\mathcal{B}}_v)$, and we assume the test spaces to be the same [15]. We introduce also an additional space $\widehat{\Lambda}$ for the Lagrange multipliers, which is either a subspace of $H^{-1/2}(\partial\widehat{\mathcal{B}}_v)$ (if $d_v = 3$) or a subspace of $H^{-1/2}(\widehat{\mathcal{B}}_v)$ (if $d_v = 2$). [16]. The weak form of a FD method reads as follows:
For all $t > 0$, find $\boldsymbol{u} \in V, p \in Q, \widehat{\boldsymbol{d}}_v \in \widehat{W}, \widehat{\boldsymbol{\lambda}} \in \widehat{\Lambda}$ such that

$$\left(\rho_f \left(\frac{\partial \boldsymbol{u}}{\partial t} + \boldsymbol{u} \cdot \nabla \boldsymbol{u}\right), \boldsymbol{v}\right) + \left(\boldsymbol{T}_f(\boldsymbol{u}, p), \nabla \boldsymbol{v}\right) + c(\widehat{\boldsymbol{\lambda}}, \boldsymbol{v} \circ \mathcal{A}_v^t) = 0 \qquad \forall \boldsymbol{v} \in V, \tag{16a}$$

$$(\nabla \cdot \boldsymbol{u}, q) = 0 \qquad \forall q \in Q, \tag{16b}$$

$$c\left(\widehat{\boldsymbol{\mu}}, \boldsymbol{u} \circ \mathcal{A}_v^t - \frac{\partial \widehat{\boldsymbol{d}}}{\partial t}\right) = 0 \qquad \forall \widehat{\boldsymbol{\mu}} \in \widehat{\Lambda}, \tag{16c}$$

$$\left((\rho_v - \rho_f)\frac{\partial^2 \widehat{\boldsymbol{d}}}{\partial t^2}, \widehat{\boldsymbol{w}}\right)_{\widehat{\mathcal{B}}_v} + \left(\widehat{\boldsymbol{T}}_s(\boldsymbol{u}, p), \nabla \widehat{\boldsymbol{w}}\right)_{\widehat{\mathcal{B}}_v} - c(\widehat{\boldsymbol{\lambda}}, \widehat{\boldsymbol{w}}) = 0 \qquad \forall \widehat{\boldsymbol{w}} \in \widehat{W}, \tag{16d}$$

where $(\cdot, \cdot)$ and $(\cdot, \cdot)_{\widehat{\mathcal{B}}_v}$ are the $L^2$-products over $\Omega$ and $\widehat{\mathcal{B}}_v$, respectively. The bilinear form $c : \widehat{\Lambda} \times \widehat{W} \to \mathbb{R}$ is such that the kinematic condition (1c) is enforced by (16c): it can be the inner product either in $L^2$ or $H^1$, or in general it can represent the duality between $H^{-1/2}$ and $H^{1/2}$ over the interface.

The Lagrange multiplier $\boldsymbol{\lambda}$ represents the stress exchanged between the blood and the moving immersed valve. In this, the class of FD methods bears some similarities with the IB class. Indeed, in [28] a classical Finite Element IB method is reformulated using Lagrange multiplier to enforce the interface conditions, and thus reinterpreted as a FD method.

The FD method originated in a different context than valve modeling [92], but it has been applied to the FSI of the AV and other cardiac valves by several groups in the past [176, 130, 13].

---

15.The generalization to the Petrov-Galerkin case would just require some additional notation

16.In much of the literature for FSI with bulk structures ($d_v = 3$), the space of Lagrange multipliers was defined over the interface. However, several works in the FD framework employed *distributed* Lagrange multipliers (see also note 10): in this case, $\widehat{\Lambda}$ is a subspace of $H^1(\widehat{\mathcal{B}}_v)$

A more recent development of the FD method takes the name of Immersogeometric method [109] and it consists in the formal replacement of the Lagrange multipliers by a Nitsche method. This method significantly reduces the complexity of the overall FSI problem, but it needs a very fine background mesh in the area spanned by the moving structure. Applications to the case of AV FSI can be found in [109, 102, 197].

The main advantage of both IB and FD methods with respect to methods with a body-fitted mesh lays in the independence between the fluid and the structure meshes. This entails that the meshes can be generated independently and that the large deformations of the valve leaflets do not induce mesh degeneration or topology changes (and thus no remeshing is ever needed). Moreover, the variational formulation of the methods circumvents the possible accuracy and stability issues associated to the interpolation of velocity and stresses between different meshes. Comparing the IB and FD strategy, an advantage of the FD formulation is that all the coupling is accounted for by the Lagrange multiplier terms, therefore, independent off-the-shelf fluid and structural solvers can be used – in principle without modifications – in a FSI iterative solution algorithm, as done in [13]. On the other hand, the introduction of Lagrange multipliers itself yields additional complexity to the overall FSI problem, related to the saddle-point nature of (16).

### 4.3 Resistive and other kinematic models

Another class of models modifies the momentum equation of the fluid problem by introducing an additional term, but instead of explicitly exchanging *stress* as done in the IB and FD approaches described above, the fluid *kinematics* in the neighborhood of the valve leaflets is imposed by a penalty term. This class is made of resistive and Brinkmann-based models, for which the fluid problem reads as follows:

$$\begin{cases} \rho_f \left( \dfrac{\partial \boldsymbol{u}}{\partial t} + \boldsymbol{u} \cdot \nabla \boldsymbol{u} \right) - \nabla \cdot \boldsymbol{T}_f(\boldsymbol{u}, p) + \mathcal{R}(\boldsymbol{u}, \boldsymbol{u}_v)\mathcal{D}_v = \boldsymbol{0} & \text{in } \Omega_f, \\ \nabla \cdot \boldsymbol{u} = 0 & \text{in } \Omega_f, \\ \text{with BC and IC,} \end{cases} \tag{17}$$

where $\mathcal{R}(\boldsymbol{u}, \boldsymbol{u}_v)$ is the penalty terms encoding the kinematic condition that the fluid velocity $\boldsymbol{u}$ has to be equal to the valve velocity $\boldsymbol{u}_v$, while $\mathcal{D}_v$ is a function whose role is to switch on this term only at the valve.

The original inspiration for these models comes from the representation of porous media immersed in the blood flow (see, e.g. [65, 7]), but then were applied to valve modeling under the assumption that very low porosity can reproduce the effects of a solid obstacle. A general classification of these models can be made in terms on whether the valve leaflets are considered as surfaces or bulk bodies:

- In *resistive* models, the thin valve leaflets are represented as surfaces and the function $\mathcal{D}_v$ is a Dirac delta, that can be sharp or smeared, thus leading to a further distinction between models. The Resistive Implicit Surface (RIS) model was devised to model a porous cerebral stent in [65] and then applied to cardiac valves in [42, 12, 181]. In this model, $\mathcal{R}(\boldsymbol{u}, \boldsymbol{u}_v) = R(\boldsymbol{u} - \boldsymbol{u}_v)$, where $R$ is a penalty constant named *resistance*, and $\mathcal{D}_v = \delta_{\Sigma_v}$ is a sharp Dirac delta distribution concentrated on the surface $\Sigma_v$ of the valve [17]. To account for this delta in the Finite Element discretization of problem (17), it is required to have a valve-conforming mesh and to manage the assembling of the mass matrix on a surface $\Sigma_v$ that is internal to the domain. On the other hand, this formulation allows sharp jumps of pressure across $\Sigma_v$, for example by doubling the degrees of freedom on the surface $\Sigma_v$ as done, e.g., in [182].
  To prevent the need for a valve-conforming mesh, the Resistive Immersed *Implicit* Surface (RIIS) model was introduced in [63] and then applied to several clinical applications [75, 76, 205, 34, 21]. In the RIIS model, the valve surface is represented implicitly as the zero-level set of a distance function $\varphi_{\Sigma_v}$, and $\mathcal{D}_v = \delta_{\Sigma_v,\varepsilon}(\varphi_{\Sigma_v})$ is a smeared Dirac delta function that goes to zero where $|\varphi| > \varepsilon$. In terms of resistance, dimensional considerations lead to define $\mathcal{R}(\boldsymbol{u}, \boldsymbol{u}_v) = \frac{R}{\varepsilon}(\boldsymbol{u} - \boldsymbol{u}_v)$, so that the resistance coefficient goes to infinity for $\varepsilon \to 0$. Leveraging the implicit level-set representation, this model does not need a valve-conforming mesh, the assembling of the Finite Element discretization is all carried out in 3D, and the fluid quantities vary smoothly (albeit with high gradients) in a $\varepsilon$-neighborhood of $\Sigma_v$.
- In *Brinkmann* models, the valve is represented as a 3D object occupying a region $\Omega_v$ and $\mathcal{D}_v$ is the binary characteristic function of $\Omega_v$. The name of these models comes directly from the Navier-Stokes-Brinkmann equations for porous media, and the resistance coefficient is expressed as $\mathcal{R}(\boldsymbol{u}, \boldsymbol{u}_v) = \frac{\mu}{K}(\boldsymbol{u} - \boldsymbol{u}_v)$ in terms of a porosity coefficient $K$ [74, 111]. A similar model, with an additional higher-order term w.r.t. $\frac{1}{K}(\boldsymbol{u} - \boldsymbol{u}_v)$ in $\mathcal{R}(\boldsymbol{u}, \boldsymbol{u}_v)$, is used in [53, 33]. In the context of valve modeling, the Finite Element approximation of these models shares with the RIIS model the non-conformity between the mesh and valve leaflets, with the boundary $\partial\Omega_v$ of the valve region treated by the volume-of-fluid method: in each mesh element, the porosity coefficient $K$ is inversely proportional to the fraction of the element volume that is occupied by the valve.

As pointed out above, both the resistive and the Brinkmann models are purely kinematic models, prescribing the blood velocity by penalization. On the other hand, the valve dynamics may either be reconstructed based on clinical imaging or modeled by a structural problem and coupled with the fluid problem by, e.g., a Dirichlet-Neumann strategy (cf. Sect. 3.2).

17.More rigorously, a Hausdorff measure of co-dimension 1

## 4.4 The family of Cut-FEM strategies

CFE methods aim to combine the geometric and physical accuracy of body-fitted methods with the flexibility of unfitted-mesh methods in treating meshes that are generated independently. To describe them, we use a similar geometric notation to that of Section 4.2: a background domain $\Omega$ is considered, containing both the fixed fluid domain $\Omega_f^t$ and the moving valve $\mathcal{B}_v^t = \mathcal{A}_v^t(\widehat{\mathcal{B}}_v)$, with corresponding meshes $\mathcal{T}_h, \mathcal{T}_{h,f}^t$, and $\mathcal{T}_{h,v}^t = \mathcal{A}_v^t(\widehat{\mathcal{T}}_{h,v})$. The FS interface conditions are defined over $\Sigma_v^t$, which denotes either the boundary $\partial\mathcal{B}_v^t$ of the valve, in the case of a 3D description, or the whole valve if a 2D surface modeling is considered. Examples of CFE methods with 2D surfaces can be found in [96, 6, 108] and for a broader discussion on CFE methods in general we refer the reader to [185].

*Remark* 1 (Fixed mesh). Although the notation $\Omega_f^t$ could lead to thinking that the fluid mesh is moving during the time evolution, we do not need to set the fluid problem in a moving-mesh framework (as in the ALE approach). Indeed, the background elements of $\mathcal{T}_h$ are fixed through time, and the time dependence is only due to the fact that $\mathcal{B}_v^t$ is moving, and thus the domain $\Omega_f^t$ is made of the following union

$$\Omega_f^t = \left( \bigcup_{K \in \mathring{\mathcal{T}}_{h,f}} K \right) \cup \left( \bigcup_{S \in \mathcal{S}_{h,f}^t} S \right),$$

where (see Fig. 4)

$$\mathring{\mathcal{T}}_{h,f} = \{K \in \mathcal{T}_h : K \cap \mathcal{B}_v^t = \emptyset\}$$
$$\mathcal{S}_{h,f}^t = \{S = K \setminus \overline{\mathcal{B}_v^t} : K \in \mathcal{T}_h \text{ and } K \cap \Sigma_v^t \neq \emptyset\}.$$

In what follows, we call *split elements* the background elements crossed by $\Sigma_v^t$:

$$\mathcal{S}_h^t = \{K \in \mathcal{T}_h : K \cap \Sigma_v^t \neq \emptyset\}.$$

At the continuous level, the equations of the problem are similar to (1a)-(1e) of the vascular FSI case, though not in the ALE framework (see Remark 1) and with $\widehat{\mathcal{B}}_v$ in the place of $\widehat{\Omega}_s$. At the discrete level, however, the background mesh does not conform with the valve, and the CFE family can be classified into a diverse set of methods. The main differences between the methods concern:

1. the discretization of the fluid on the elements of the background mesh that are crossed by the fluid-solid interface;
2. the imposition of the FSI interface conditions.

Regarding the first point, the difficulty lies in that $\mathcal{S}_{h,f}^t$ is made of polyhedra with a generic number of faces, as shown in the pink elements of Fig. 4, on which the classical continuous Finite Element method is hardly applicable. Two classes of methods address this issue in dual ways:

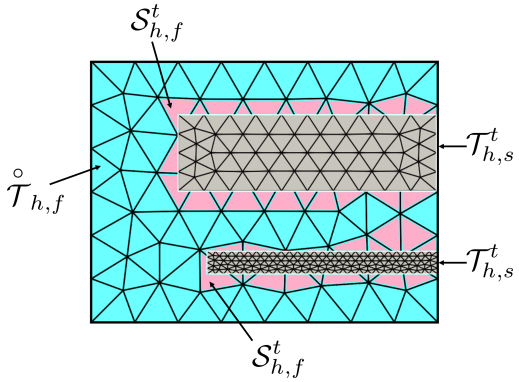


**FIGURE 4** Meshes of the CFE methods, in the case of a thick (above) and thin (below) structure: in grey the structure mesh $\mathcal{T}^t_{h,s}$; in blue the mesh $\mathring{\mathcal{T}}_{h,f}$ far from the structure; in pink the fluid portion $\mathcal{S}^t_{h,f}$ of the split elements.

- The Polygonal/Polyhedral Discontinuous Galerkin (PolyDG) method [126, 9], first applied to 2D FSI problems in [8, 206], is based on function spaces generated by *modal* basis functions based on bounding boxes of the mesh elements [44]. Therefore, the computational mesh is allowed to contain polygonal/polyhedral elements with arbitrary numbers of edges/faces. In this method, each portion of the split elements is a valid element on its own, therefore $\mathcal{T}^t_{h,f,pDG} = \mathring{\mathcal{T}}^t_{h,f} \cup \mathcal{S}^t_{h,f}$ is a valid mesh and the continuity of the solution in all $\Omega^t_f$ is enforced weakly with standard DG terms in the fluid problem.
- Alternatively, the eXtended Finite Element Method (XFEM) employs a computational mesh $\mathcal{T}^t_{h,f,XFEM} = \mathring{\mathcal{T}}^t_{h,f} \cup \mathcal{S}^t_h$ made only of the original tetrahedra (or hexahedra). The trial and test function spaces are then built by extending the standard Finite Element spaces over $\mathring{\mathcal{T}}^t_{h,f}$ with additional degrees of freedom (dofs) over the split elements $\mathcal{S}^t_h$, with different purposes depending on the thickness of the structure. In the case of *thick* structures, namely structures whose thickness is larger than the size $h$ of the background elements, the Finite Element basis functions corresponding to the new dofs for each $K \in \mathcal{S}^t_h$ are multiplied by enrichment functions encoding the restriction of the problem formulation on $K \cap \Omega^t_f$ (see, e.g., [83, 84, 140, 127]). If, instead, a *thin* structure is considered, with a thickness smaller than $h$ – or also if the structure is a 2D surface immersed in a 3D domain – each split element can have more than one connected component in $\Omega^t_f$, and all the new dofs are duplicated to allow each of these components to have a full set of dofs on which to assemble the fluid problem (see, e.g., [167, 207, 185, 66]). In this latter case, additional constraints have to be introduced to enforce the continuity of

the fluid solution among the split elements on the same side of the structure: this is typically done by DG-based Nitsche mortaring, which requires the introduction of additional terms both in the fluid and in the structure solver.

Due to the motion of the valve, the fluid portion of the split elements may be extremely small. This can undermine the stability of the XFEM, thus ad-hoc stabilization strategies have to be adopted, such as the ghost penalty stabilization [37]. On the other hand, the stability of the PolyDG method has been theoretically proven independently of the size of the elements, under mild assumptions, and its robustness w.r.t. element anisotropy has been numerically assessed [8].

Concerning the imposition of interface conditions (point 2 above), all the works mentioned above considered a Nitsche method based on DG mortaring assembled directly on the faces of the interface $\Sigma_v^t$. A similar strategy was considered also in the case of other methods, like the Interior-Penalty Finite Element Method (bearing many similarities with the XFEM) [123, 122, 203] or the unfitted version of the Hybrid High-Order method (allowing the use of generic polyhedral elements) [59, 38]. A variation was proposed in [139], where an additional body-fitted fluid mesh surrounding $\mathcal{B}_v^t$ was introduced to accurately capture the boundary layer and compute boundary stresses, in a similar fashion to Chimera methods; in this case, the mortaring was assembled on the interface between this additional mesh and the background mesh. Another alternative to assembling the Nitsche terms on $\Sigma_v^t$ was introduced as the Shifted Boundary Method [134, 133], where the interface conditions are projected onto the closest faces of the fluid mesh, thus preventing the need of element cutting. Other variational approaches employed, instead, Lagrange multipliers on the interface (similarly to the FD approach of Section 4.2) [83, 110].

## 5 CRITICAL ISSUES IN AORTIC FSI SIMULATION

In this section, we want to give very short hints about some critical issues arising when one wants to realize patient-specific FSI numerical simulations in the aorta. For the sake of exposition, we limit this overview to the vascular case. We stress that with "patient-specific" we do not mean only the use of geometric data coming from medical images but also personalized model parameters and boundary conditions.

### 5.1 The issue of boundary conditions

We start with the fluid problem. Regarding the inlet $\Gamma_{in}^t$ of the aortic domain, we can in general recognize the following approaches to prescribe significant boundary conditions:

- Prescribe data coming from measures, e.g.:
  i) Velocity data $\boldsymbol{g}$ coming from PC-MRI or 4DFlow acquisitions, allowing to prescribe a Dirichlet condition $\boldsymbol{u} = \boldsymbol{g}$ on $\Gamma_{in}^t$, see, e.g, [47];

ii) Flow rate data $Q(t)$ coming from EchoColor Doppler or PC-MRI acquisitions. This gives the *defective* condition

$$\int_{\Gamma_{in}^t} \boldsymbol{u} \cdot \boldsymbol{n} = Q,$$

which needs to be completed either with some assumption on the velocity profile (e.g. flat [142, 30]) or, under the assumption of null tangential stress or velocity, with some more mathematically sound methods, such as Lagrange multipliers, optimal control, or Nitsche [71];
iii) Pressure data $P$. Owing to the reasonable assumption of constant pressure over a section orthogonal to the longitudinal axis and the predominance of pressure over viscous stresses on such a section, often this data is prescribed by means of the following Neumann condition:

$$\boldsymbol{T}_f(\boldsymbol{u}, p)\boldsymbol{n} = P\boldsymbol{n} \qquad \text{on } \Gamma_{in}^t;$$

- Coupling the aorta FSI model with an *electro-mechano-fluid* (EMF) model of the left ventricle [166, 177, 34]. This allows to set proper interface inlet conditions at the aortic valve plane (continuity of mass and tractions) which, in case of splitting between the cardiac and the vessel model, provide inlet boundary conditions on the velocity or pressure[18].

Regarding the outlets $\Gamma_{out}^t$ (usually the entrance of the iliac arteries, a section located at the abdominal level, the supra-aortic arteries), we can in principle detect three strategies to prescribe proper boundary conditions:

- The coupling with a 1D reduced FSI model representing the distal systemic circulation (or a part of it), obtained by integrating the FSI equations over a section $S$ and under suitable simplifying hypotheses [152]. This leads to a hyperbolic system of two equations in the unknowns area $A = A(t, z)$ of $S$ and flow rate $Q = Q(t, z)$ over $S$, $z$ being the axial coordinate. Writing the interface conditions between the 3D and 1D FSI models, stating the continuity of mass and tractions, and using a partitioned procedure, one obtains suitable boundary conditions for the 3D model in terms of flow rate or mean pressure conditions [160]. This strategy is particularly suited when the outlet is located at a section at the abdominal level [135] or at the entrance of the iliac arteries [24];
- The coupling with a *Windkessel* model, i.e. a lumped parameter (0D) model accounting in a synthetic way for the overall resistance and compliance of the distal circulatory system. The most simple Windkessel element is formed by two resistances and one capacitance [160]. Again, the splitting between 3D and 0D models may provide suitable boundary conditions at the 3D outlet; sometimes the 0D model has been directly inserted in the 3D model

18.In the case a 0D fluid model is used in the EMF model, the inlet condition will be defective

as boundary condition [187]. The use of a Windkessel model is suited for the main aortic outlets [43] and also for the supra-aortic arteries [156];

- It is well known that when pressure data (although coming from the literature) is prescribed at a FSI outlet, spurious numerical pressure wave reflections may occur [72]. To overcome this, it has been proposed to use *absorbing* boundary conditions obtained by annihilating the incoming characteristic variable of a "condensed" 1D model [150]. This leads to a resistance boundary condition (i.e. a linear combination between flow rate and mean traction) for the normal component, e.g. from [149] we have

$$\frac{1}{|\Gamma^t_{out}|}\int_{\Gamma^t_{out}} \boldsymbol{T}_f\boldsymbol{n}\cdot\boldsymbol{n} - R\int_{\Gamma^t_{out}} \boldsymbol{u}\cdot\boldsymbol{n} = P_{ext} \qquad R=\sqrt{\frac{\rho_f E H_s \pi}{2(1-\nu^2)A_0^{7/4}}},$$

with $A_0$ the section area at time 0 and $P_{ext}$ the external pressure. The flow rate term could be treated explicitly, leading in fact to a standard Neumann condition (see point iii above). Although not completely representing the physiological conditions, since physiological pressure wave reflections are dumped, this simple strategy allows at least to recover a reasonable solution without spurious reflections.

As for the structure and fluid mesh problems, one often prescribes either homogeneous Dirichlet conditions at the inlet/outlets, corresponding to fixing the geometries, or mixed homogeneous Dirichlet (for the normal direction) and Neumann (for the tangential directions) conditions, allowing deformation in the tangential directions. At the external surface $\Gamma^t_{ext}$, it is crucial to set proper boundary conditions accounting for the surrounding tissue in order to preserve stability and obtain accurate results. This is usually done by prescribing a Robin condition surrogating the elastic response of the surrounding tissue by means of a simple linear local model:

$$\gamma_{ST}\widehat{\boldsymbol{d}} + \widehat{\boldsymbol{T}}_s(\widehat{\boldsymbol{d}}) = P_{ext}\widehat{\boldsymbol{n}} \qquad \text{on } \widehat{\Gamma}_{ext},$$

where $\gamma_{ST} = \gamma_{ST}(\boldsymbol{x})$ represents the elastic properties of the surrounding tissue [142].

## 5.2 Recovering the unloaded geometric configuration

Standard medical images usually used to obtain the aortic computational domain (such as MRI and CT) given an average information of the geometry during the heartbeat, often corresponding to the diastolic configuration. More advanced acquisition techniques, such as cineMRI and dynamic CT, allow to have many geometric configurations (about 20) per heartbeat. In any case, the unloaded configuration (i.e. the empty one, without blood inside) is unknown, since the reconstructed geometry refers to a state corresponding to a non-null blood pressure ($P_m \simeq 70$ mmHg). The knowledge of the unloaded configuration is

however necessary when a non-linear material is considered for the vessel wall mechanics, to work at the right stress/strain point or, in other words, to have the right prestress in the artery.

To recover the zero-pressure configuration and the in vivo stress tensor field, in [161] the authors proposed an optimization problem where the unknown unloaded configuration $\boldsymbol{X}^*$ is found as

$$\boldsymbol{X}^* = \boldsymbol{x}_m - \kappa \boldsymbol{U},$$

for a suitable parameter $\kappa$, where $\boldsymbol{x}_m$ is the image-based configuration and $\boldsymbol{U}$ is the displacement of a forward simulation applied to the image-based configuration loaded by $P_m$. To determine $\kappa$, an optimization procedure is performed in the range $\kappa \in [0.5, 2]$ with the aim of minimizing the discrepancy between $\boldsymbol{X}^*$ and $\boldsymbol{x}_\kappa$, where the latter is obtained by loading $\boldsymbol{X}^*$ by $P_m$. This method has been successfully applied to an AAA configuration. In [29], a fixed-point alternative has been proposed, where a displacement $\boldsymbol{U}_{(k)}$ is found at each iteration $k$ by solving a forward structural problem, where the configuration $\boldsymbol{X}_{(k-1)}$ found at iteration $k-1$ is used as reference and loaded by $P_m$. Such displacement is then subtracted from the original image-based configuration to find the new geometry at iteration $k$:

$$\boldsymbol{X}_{(k)} = \boldsymbol{x}_m - \boldsymbol{U}_{(k)}.$$

This method has been applied to the case of an aorta of a mouse. Another method based on the backward application of computed forward deformations is reported in [54].

Instead of computing explicitly the zero-pressure configuration as proposed in the above papers, a different approach is based on computing the in-vivo prestress to be applied to the reference image-based configuration. This is done by an iterative procedure in which the external pressure is gradually incremented up to $P_m$. Correspondingly, incremental structure problems are solved until equilibrium, using a multiplicative decomposition of the deformation gradient

$$\boldsymbol{F}_{(k+1)} = \widetilde{\boldsymbol{F}}_{(k+1)} \boldsymbol{F}_{(k)},$$

where $\widetilde{\boldsymbol{F}}_{(k+1)}$ is found by using the previous Jacobian [81, 79]. This strategy was successfully applied to the case of AAA geometries.

## 5.3 FSI parameter calibration & validation

Probably, the main challenging issue today related to the numerical solution of FSI problems for the aorta is given by the calibration of the model parameters, in order to make the simulation patient-specific. This is crucial for the structure problem since there is a high inter-subjects and intra-subject variability of the (healthy and damaged) vessel wall mechanical properties, such as the parameters describing the compressibility (e.g. the Poisson ratio) and the elastic behavior (e.g. the Young modulus).

A first group of works aimed at using physical principles in combination with medical data in the aorta in order to calibrate the structural parameters. For example, in [5] the authors proposed to estimate the pulse wave velocity $c$ and then to approximate the Young modulus as

$$E = \frac{3\rho_f c^2 \sqrt{A_0}}{2H_s\sqrt{\pi}}.$$

To estimate $c$ it is possible to start from two PC-MRI flow rate acquisitions (a proximal and a distal one) and to measure the delay of the latter in correspondence with the transit time of the foot of the flow waveforms. In order to have a non-uniform in space $c$, if also area waveforms are available, an alternative method relies on estimating $c$ at different aortic levels and then to apply a least-square fitting to find $\xi$ such that $c = \xi D_d^{-1/2}$, where $D_d$ is the diastolic diameter [4]. Regarding the three parameters $R_1, R_2, C$ of a three-element Windkessel outflow model, we can estimate first the total peripheral resistance as

$$R_1 + R_2 = \frac{\frac{1}{T}\int_0^T P(t)}{\frac{1}{T}\int_0^T Q(t)},$$

with $P$ and $Q$ available waveforms data of pressure and flow rate, see [163]. Then, the resistance of the large vessels $R_1$ can be estimated by $R_1 = \frac{c\rho_f}{A}$ [196, 3]. For the compliance $C$, see, e.g. [106].

Another group of studies proposed to directly estimate the parameters by a fitting with available data, using the minimization of a suitable functional; regarding applications to the aorta with real medical data, see, e.g., [43, 163] for the estimation of Windkessel parameters, [184] for the elastic properties calibration, and [143] for the surrounding tissue.

Finally, we refer to works that focused more on the numerical strategy to efficiently solve the calibration problem, often tested only with synthetic data. We mention studies that build the adjoint FSI problem to solve an optimization problem for the calibration of the elastic properties [153] or the Windkessel parameters [105]; algorithms based on the Kalman filter procedure, adapted to the non-linear case, see, e.g. [22, 23] for the calibration of elastic properties; recent methods based on *machine learning*, see [128] for the elastic properties.

Related to the calibration issue is that of the validation of the FSI model and corresponding numerical strategies. This could be done in general by comparing the numerical results with medical image-based data, in terms of blood velocity and pressure and vessel displacements. In principle, a fair validation should be obtained by using data for the comparison that have not been already used for calibration nor for boundary conditions. For validation of blood velocity, we mention, among the others, [120] for the healthy aorta against PC-MRI measures, [165, 155] for aortic coarctation and Marfan patients, respectively, against 4DFlow MRI measures.

Other studies validated their FSI model against in-vitro measures: we mention, e.g., [48] for a validation of blood velocity in idealized aortas with dissection against ultrasound in vitro measurements, [114] for a validation of vessel displacements in idealized abdominal aortic aneurysms against T-4 ultrasound echo track measures, and [46] for a validation of a strategy to recover the unloaded aortic configuration.

# Bibliography


[1] Syed Samar Abbas, Mohammad Shakir Nasif, and Rafat Al-Waked. "State-of-the-art numerical fluid–structure interaction methods for aortic and mitral heart valves simulations: A review". In: *Simulation* 98.1 (2022), pp. 3–34.

[2] Arian Aghilinejad et al. "Model-Based Fluid-Structure Interaction Approach for Evaluation of Thoracic Endovascular Aortic Repair Endograft Length in Type B Aortic Dissection". In: *Frontiers in Bioengineering and Biotechnology* 10 (2022).

[3] Jordi Alastruey et al. "Lumped parameter outflow models for 1-D blood flow simulations: effect on pulse waves and parameter estimation". In: *Communications in Computational Physics* 4.2 (2008), pp. 317–336.

[4] Jordi Alastruey et al. "Modelling pulse wave propagation in the rabbit systemic circulation to assess the effects of altered nitric oxide synthesis". In: *Journal of Biomechanics* 42.13 (2009), pp. 2116–2123.

[5] Jordi Alastruey et al. "On the impact of modelling assumptions in multi-scale, subject-specific models of aortic haemodynamics". In: *Journal of The Royal Society Interface* 13.119 (2016), p. 20160073.

[6] Frédéric Alauzet et al. "Nitsche-XFEM for the coupling of an incompressible fluid with immersed thin-walled structures". In: *Computer Methods in Applied Mechanics and Engineering* 301 (2016), pp. 300–335.

[7] Philippe Angot, Charles-Henri Bruneau, and Pierre Fabrie. "A penalization method to take into account obstacles in incompressible viscous flows". In: *Numerische Mathematik* 81.4 (1999), pp. 497–520.

[8] Paola Antonietti et al. "Numerical solution of fluid-structure interaction problems by means of a high order Discontinuous Galerkin method on polygonal grids". In: *Finite Elements in Analysis and Design* 159 (2019), pp. 1–14.

[9] PF Antonietti and I Mazzieri. "High-order discontinuous Galerkin methods for the elastodynamics equation on polygonal and polyhedral meshes". In: *Computer Methods in Applied Mechanics and Engineering* 342 (2018), pp. 414–437.

[10] Hossein Asadi, Mohammadali Hedayat, and Iman Borazjani. "The Effects of Implantation Orientation of a Bileaflet Mechanical Heart Valve in an Anatomic Left Ventricle-Aorta Configuration". In: *Journal of Biomechanical Engineering* 144.10 (2022), p. 101008.

[11] Matteo Astorino, Franz Chouly, and Miguel A Fernández. "Robin based semi-implicit coupling in fluid-structure interaction: Stability analysis and numerics". In: *SIAM Journal on Scientific Computing* 31.6 (2010), pp. 4041–4065.

[12] Matteo Astorino et al. "A robust and efficient valve model based on resistive immersed surfaces". In: *International Journal for Numerical Methods in Biomedical Engineering* 28.9 (2012), pp. 937–959.

[13] Matteo Astorino et al. "Fluid–structure interaction and multi-body contact: application to aortic valves". In: *Computer Methods in Applied Mechanics and Engineering* 198.45-46 (2009), pp. 3603–3612.

[14] Santiago Badia, Fabio Nobile, and Christian Vergara. "Fluid–structure partitioned procedures based on Robin transmission conditions". In: *Journal of Computational Physics* 227.14 (2008), pp. 7027–7051.

[15] Santiago Badia, Fabio Nobile, and Christian Vergara. "Robin–Robin preconditioned Krylov methods for fluid–structure interaction problems". In: *Computer Methods in Applied Mechanics and Engineering* 198.33-36 (2009), pp. 2768–2784.

[16] Santiago Badia, Annalisa Quaini, and Alfio Quarteroni. "Modular vs. non-modular preconditioners for fluid–structure systems with large added-mass effect". In: *Computer Methods in Applied Mechanics and Engineering* 197.49-50 (2008), pp. 4216–4232.

[17] Santiago Badia, Annalisa Quaini, and Alfio Quarteroni. "Splitting methods based on algebraic factorization for fluid-structure interaction". In: *SIAM Journal on Scientific Computing* 30.4 (2008), pp. 1778–1805.

[18] Theodorus MJ van Bakel et al. "Cardiac remodelling following thoracic endovascular aortic repair for descending aortic aneurysms". In: *European Journal of Cardio-Thoracic Surgery* 55.6 (2019), pp. 1061–1070.

[19] Kathrin Bäumler et al. "Fluid–structure interaction simulations of patient-specific aortic dissection". In: *Biomechanics and modeling in mechanobiology* 19.5 (2020), pp. 1607–1628.

[20] Barna Becsek, Leonardo Pietrasanta, and Dominik Obrist. "Turbulent systolic flow downstream of a bioprosthetic aortic valve: velocity spectra, wall shear stresses, and turbulent dissipation rates". In: *Frontiers in physiology* 11 (2020), p. 577188.

[21] Lorenzo Bennati et al. "An image-based computational fluid dynamics study of mitral regurgitation in presence of prolapse". In: *Submitted. MOX Report 18/2022* (2022).

[22] Cristóbal Bertoglio, Philippe Moireau, and Jean-Frederic Gerbeau. "Sequential parameter estimation for fluid–structure problems: application to hemodynamics". In: *International Journal for Numerical Methods in Biomedical Engineering* 28.4 (2012), pp. 434–455.

[23] Cristóbal Bertoglio et al. "Identification of artery wall stiffness: In vitro validation and in vivo results of a data assimilation procedure applied to a 3D fluid–structure interaction model". In: *Journal of Biomechanics* 47.5 (2014), pp. 1027–1034.

[24] PJ Blanco, SA Urquiza, and RA Feijóo. "Assessing the influence of heart rate in local hemodynamics through coupled 3D-1D-0D models". In: *International Journal for Numerical Methods in Biomedical Engineering* 26.7 (2010), pp. 890–903.

[25] D. Boffi and L Gastaldi. "A finite element approach for the immersed boundary method". In: *Computers & Structures* 81.8-11 (2003). K.J Bathe 60th Anniversary Issue, pp. 491–501. ISSN: 0045-7949. DOI: http://dx.doi.org/10.1016/S0045-7949(02)00404-2. URL: http://www.sciencedirect.com/science/article/pii/S0045794902004042.

[26] D. Boffi, L. Gastaldi, and L. Heltai. "Numerical stability of the finite element immersed boundary method". In: *Mathematical Models and Methods in Applied Sciences* 17.10 (2007), pp. 1479–1505.

[27] D. Boffi et al. "On the hyper-elastic formulation of the immersed boundary method". In: *Computer Methods in Applied Mechanics and Engineering* 197(25–28) (2008), pp. 2210–2231.

[28] Daniele Boffi and Lucia Gastaldi. "A fictitious domain approach with Lagrange multiplier for fluid-structure interactions". In: *Numerische Mathematik* 135.3 (2017), pp. 711–732.

[29] Joris Bols et al. "A computational method to assess the in vivo stresses and unloaded configuration of patient-specific blood vessels". In: *Journal of computational and Applied mathematics* 246 (2013), pp. 10–17.

[30] Diana Bonomi et al. "Influence of the aortic valve leaflets on the fluid-dynamics in aorta in presence of a normally functioning bicuspid valve". In: *Biomechanics and modeling in mechanobiology* 14.6 (2015), pp. 1349–1361.

[31] Iman Borazjani. "Fluid–structure interaction, immersed boundary-finite element method simulations of bio-prosthetic heart valves". In: *Computer Methods in Applied Mechanics and Engineering* 257 (2013), pp. 103–116.

[32] Iman Borazjani, Liang Ge, and Fotis Sotiropoulos. "Curvilinear immersed boundary method for simulating fluid structure interaction with complex 3D rigid bodies". In: *Journal of Computational physics* 227.16 (2008), pp. 7587–7620.

[33] Jochen Brenneisen et al. "Sequential coupling shows minor effects of fluid dynamics on myocardial deformation in a realistic whole-heart model". In: *Frontiers in Cardiovascular Medicine* (2021), p. 1967.

[34] Michele Bucelli et al. "A mathematical model that integrates cardiac electrophysiology, mechanics and fluid dynamics: application to the human left heart". In: *arXiv preprint arXiv:2208.05551* (2022).

[35] M Bukač et al. "A modular, operator-splitting scheme for fluid–structure interaction problems with thick structures". In: *International journal for numerical methods in fluids* 74.8 (2014), pp. 577–604.

[36] Martina Bukač et al. "Time-adaptive partitioned method for fluid-structure interaction problems with thick structures". In: *Journal of Computational Physics* 473 (2023), p. 111708.

[37] Erik Burman. "Ghost penalty". In: *Comptes Rendus Mathematique* 348.21-22 (2010), pp. 1217–1220.

[38] Erik Burman, Guillaume Delay, and Alexandre Ern. "An unfitted hybrid high-order method for the Stokes interface problem". In: *IMA Journal of Numerical Analysis* 41.4 (2021), pp. 2362–2387.

[39] Erik Burman, Rebecca Durst, and Johnny Guzmán. "Stability and error analysis of a splitting method using Robin–Robin coupling applied to a fluid–structure interaction problem". In: *Numerical Methods for Partial Differential Equations* 38.5 (2022), pp. 1396–1406.

[40] Erik Burman and Miguel A Fernández. "Explicit strategies for incompressible fluid-structure interaction problems: Nitsche type mortaring versus Robin–Robin coupling". In: *International Journal for Numerical Methods in Engineering* 97.10 (2014), pp. 739–758.

[41] Erik Burman and Miguel A Fernández. "Stabilization of explicit coupling in fluid–structure interaction involving fluid incompressibility". In: *Computer Methods in Applied Mechanics and Engineering* 198.5-8 (2009), pp. 766–784.

[42] Alfonso Caiazzo, Miguel A Fernández, and Vincent Martin. "Analysis of a stabilized finite element method for fluid flows through a porous interface". In: *Applied Mathematics Letters* 24.12 (2011), pp. 2124–2127.

[43] Rossella Campobasso et al. "Evaluation of peak wall stress in an ascending thoracic aortic aneurysm using FSI simulations: effects of aortic stiffness and peripheral resistance". In: *Cardiovascular engineering and technology* 9.4 (2018), pp. 707–722.

[44] Andrea Cangiani, Emmanuil H Georgoulis, and Paul Houston. "hp-version discontinuous Galerkin methods on polygonal and polyhedral meshes". In: *Mathematical Models and Methods in Applied Sciences* 24.10 (2014), pp. 2009–2041.

[45] Paola Causin, Jean-Frédéric Gerbeau, and Fabio Nobile. "Added-mass effect in the design of partitioned algorithms for fluid–structure problems". In: *Computer methods in applied mechanics and engineering* 194.42-44 (2005), pp. 4506–4527.

[46] Santanu Chandra et al. "A methodology for the derivation of unloaded abdominal aortic aneurysm geometry with experimental validation". In: *Journal of biomechanical engineering* 138.10 (2016).

[47] Santanu Chandra et al. "Fluid-structure interaction modeling of abdominal aortic aneurysms: the impact of patient-specific inflow conditions and fluid/solid coupling". In: *Journal of biomechanical engineering* 135.8 (2013).

[48] HY Chen et al. "Editor's Choice–Fluid–Structure Interaction Simulations of Aortic Dissection with Bench Validation". In: *European Journal of Vascular and Endovascular Surgery* 52.5 (2016), pp. 589–595.

[49] Mei Yan Chong et al. "Effect of intimal flap motion on flow in acute type B aortic dissection by using fluid-structure interaction". In: *International journal for numerical methods in biomedical engineering* 36.12 (2020), e3399.

[50] Ramon Codina et al. "The fixed-mesh ALE approach for the numerical approximation of flows in moving domains". In: *Journal of computational Physics* 228.5 (2009), pp. 1591–1611.

[51] Claudia Maria Colciago, Simone Deparis, and Alfio Quarteroni. "Comparisons between reduced order models and full 3D models for fluid–structure interaction problems in haemodynamics". In: *Journal of Computational and Applied Mathematics* 265 (2014), pp. 120–138.

[52] Paolo Crosetto et al. "Parallel algorithms for fluid-structure interaction problems in haemodynamics". In: *SIAM Journal on Scientific Computing* 33.4 (2011), pp. 1598–1622.

[53] Anna Daub, Jochen Kriegseis, and Bettina Frohnapfel. "Replication of left ventricular haemodynamics with a simple planar mitral valve model". In: *Biomedical Engineering/Biomedizinische Technik* 65.5 (2020), pp. 595–603.

[54] S De Putter et al. "Patient-specific initial wall stress in abdominal aortic aneurysms with a backward incremental method". In: *Journal of biomechanics* 40.5 (2007), pp. 1081–1090.

[55] Joris Degroote, Klaus-Jürgen Bathe, and Jan Vierendeels. “Performance of a new partitioned procedure versus a monolithic procedure in fluid–structure interaction”. In: *Computers & Structures* 87.11-12 (2009), pp. 793–801.

[56] Simone Deparis et al. “FaCSI: A block parallel preconditioner for fluid–structure interaction in hemodynamics”. In: *Journal of Computational Physics* 327 (2016), pp. 700–718.

[57] Simone Deparis et al. “Fluid–structure algorithms based on Steklov–Poincaré operators”. In: *Computer Methods in Applied Mechanics and Engineering* 195.41-43 (2006), pp. 5797–5812.

[58] Wulf G Dettmer et al. “New iterative and staggered solution schemes for incompressible fluid-structure interaction based on Dirichlet-Neumann coupling”. In: *International Journal for Numerical Methods in Engineering* 122.19 (2021), pp. 5204–5235.

[59] Daniele A Di Pietro and Alexandre Ern. “A hybrid high-order locking-free method for linear elasticity on general meshes”. In: *Computer Methods in Applied Mechanics and Engineering* 283 (2015), pp. 1–21.

[60] J. Donea. “An arbitrary Lagrangian-Eulerian finite element method for transient dynamic fluid-structure interaction”. In: *Computer Methods in Applied Mechanics and Engineering* 33 (1982), pp. 689–723.

[61] Howard Elman et al. “Block preconditioners based on approximate commutators”. In: *SIAM Journal on Scientific Computing* 27.5 (2006), pp. 1651–1668.

[62] Monica Emendi et al. “Patient-specific bicuspid aortic valve biomechanics: a magnetic resonance imaging integrated fluid–structure interaction approach”. In: *Annals of biomedical engineering* 49.2 (2021), pp. 627–641.

[63] Marco Fedele et al. “A patient-specific aortic valve model based on moving resistive immersed implicit surfaces”. In: *Biomechanics and Modeling in Mechanobiology* 16.5 (2017), pp. 1779–1803.

[64] Yong Feng et al. “Computational modeling for surgical reconstruction of aortic valve by using autologous pericardium”. In: *IEEE Access* 8 (2020), pp. 97343–97352.

[65] Miguel A Fernández, Jean-Frédéric Gerbeau, and Vincent Martin. “Numerical simulation of blood flows through a porous interface”. In: *ESAIM: Mathematical Modelling and Numerical Analysis* 42.6 (2008), pp. 961–990.

[66] Miguel A Fernández and Fannie M Gerosa. “An unfitted mesh semi-implicit coupling scheme for fluid-structure interaction with immersed solids”. In: *International Journal for Numerical Methods in Engineering* 122.19 (2021), pp. 5384–5408.

[67] Miguel A Fernández, Jimmy Mullaert, and Marina Vidrascu. "Generalized Robin–Neumann explicit coupling schemes for incompressible fluid-structure interaction: Stability analysis and numerics". In: *International Journal for Numerical Methods in Engineering* 101.3 (2015), pp. 199–229.

[68] Miguel Angel Fernández, J-F Gerbeau, and Céline Grandmont. "A projection semi-implicit scheme for the coupling of an elastic structure with an incompressible fluid". In: *International Journal for Numerical Methods in Engineering* 69.4 (2007), pp. 794–821.

[69] Miguel Angel Fernández and Marwan Moubachir. "A Newton method using exact Jacobians for solving fluid–structure coupling". In: *Computers & Structures* 83.2-3 (2005), pp. 127–142.

[70] C Alberto Figueroa et al. "A coupled momentum method for modeling blood flow in three-dimensional deformable arteries". In: *Computer methods in applied mechanics and engineering* 195.41-43 (2006), pp. 5685–5706.

[71] Luca Formaggia and Christian Vergara. "Prescription of general defective boundary conditions in fluid-dynamics". In: *Milan Journal of Mathematics* 80.2 (2012), pp. 333–350.

[72] Luca Formaggia et al. "On the coupling of 3D and 1D Navier–Stokes equations for flow problems in compliant vessels". In: *Computer methods in applied mechanics and engineering* 191.6-7 (2001), pp. 561–582.

[73] Christiane Förster, Wolfgang A Wall, and Ekkehard Ramm. "Artificial added mass instabilities in sequential staggered coupling of nonlinear structures and incompressible viscous flows". In: *Computer methods in applied mechanics and engineering* 196.7 (2007), pp. 1278–1293.

[74] Jana Fuchsberger et al. "On the incorporation of obstacles in a fluid flow problem using a Navier–Stokes–Brinkman penalization approach". In: *Journal of Computational Science* 57 (2022), p. 101506.

[75] Ivan Fumagalli et al. "An image-based computational hemodynamics study of the Systolic Anterior Motion of the mitral valve". In: *Computers in Biology and Medicine* 123 (2020), p. 103922.

[76] Ivan Fumagalli et al. "Image-based computational hemodynamics analysis of systolic obstruction in hypertrophic cardiomyopathy". In: *Frontiers in Physiology* (2022), p. 2437.

[77] Martin J Gander. "Optimized schwarz methods". In: *SIAM Journal on Numerical Analysis* 44.2 (2006), pp. 699–731.

[78] Liang Ge and Fotis Sotiropoulos. "A numerical method for solving the 3D unsteady incompressible Navier–Stokes equations in curvilinear domains with complex immersed boundaries". In: *Journal of computational physics* 225.2 (2007), pp. 1782–1809.

[79] Michael W Gee, Ch Förster, and WA Wall. "A computational strategy for prestressing patient-specific biomechanical problems under finite deformation". In: *International Journal for Numerical Methods in Biomedical Engineering* 26.1 (2010), pp. 52–72.

[80] Michael W Gee, Ulrich Küttler, and WA2796873 Wall. "Truly monolithic algebraic multigrid for fluid–structure interaction". In: *International Journal for Numerical Methods in Engineering* 85.8 (2011), pp. 987–1016.

[81] MW Gee et al. "Prestressing in finite deformation abdominal aortic aneurysm simulation". In: *Journal of biomechanics* 42.11 (2009), pp. 1732–1739.

[82] Luca Gerardo-Giorda, Fabio Nobile, and Christian Vergara. "Analysis and optimization of Robin–Robin partitioned procedures in fluid-structure interaction problems". In: *SIAM Journal on Numerical Analysis* 48.6 (2010), pp. 2091–2116.

[83] A. Gerstenberger. "An XFEM based fixed-grid approach to fluid-structure interaction". PhD thesis. Technical University of Munich, 2010.

[84] A. Gerstenberger and W. A. Wall. "An embedded Dirichlet formulation for 3D continua". In: *International Journal for Numerical Methods in Engineering* 82.5 (2010), pp. 537–563.

[85] Ram P Ghosh et al. "Numerical evaluation of transcatheter aortic valve performance during heart beating and its post-deployment fluid–structure interaction analysis". In: *Biomechanics and modeling in mechanobiology* 19.5 (2020), pp. 1725–1740.

[86] Giacomo Gigante, Matteo Pozzoli, and Christian Vergara. "Optimized Schwarz methods for the diffusion-reaction problem with cylindrical interfaces". In: *SIAM Journal on Numerical Analysis* 51.6 (2013), pp. 3402–3430.

[87] Giacomo Gigante, Giulia Sambataro, and Christian Vergara. "Optimized Schwarz methods for spherical interfaces with application to fluid-structure interaction". In: *SIAM Journal on Scientific Computing* 42.2 (2020), A751–A770.

[88] Giacomo Gigante and Christian Vergara. "Analysis and optimization of the generalized Schwarz method for elliptic problems with application to fluid–structure interaction". In: *Numerische Mathematik* 131.2 (2015), pp. 369–404.

[89] Giacomo Gigante and Christian Vergara. "On the choice of interface parameters in Robin–Robin loosely coupled schemes for fluid–structure interaction". In: *Fluids* 6.6 (2021), p. 213.

[90] Giacomo Gigante and Christian Vergara. “On the stability of a loosely-coupled scheme based on a Robin interface condition for fluid-structure interaction”. In: *Computers & Mathematics with Applications* 96 (2021), pp. 109–119.

[91] Anvar Gilmanov et al. “Image-guided fluid-structure interaction simulation of transvalvular hemodynamics: Quantifying the effects of varying aortic valve leaflet thickness”. In: *Fluids* 4.3 (2019), p. 119.

[92] R. Glowinski, T.-W. Pan, and J. Periaux. “A fictitious domain method for Dirichlet problem and applications”. In: *Computer Methods in Applied Mechanics and Engineering* 111.3-4 (1994), pp. 283–303.

[93] B. E. Griffith. “Immersed boundary model of aortic heart valve dynamics with physiological driving and loading conditions”. In: *International Journal for Numerical Methods in Biomedical Engineering* 28.3 (2012), pp. 317–345.

[94] B.E. Griffith et al. “Simulating the fluid dynamics of natural and prosthetic heart valves using the immersed boundary method”. In: *International Journal of Applied Mechanics* 1 (2009), pp. 137–176.

[95] S Haeri and JS Shrimpton. “On the application of immersed boundary, fictitious domain and body-conformal mesh methods to many particle multiphase flows”. In: *International Journal of Multiphase Flow* 40 (2012), pp. 38–55.

[96] P. Hansbo, M. G. Larson, and S. Zahedi. “Characteristic cut finite element methods for convection–diffusion problems on time dependent surfaces”. In: *Computer Methods in Applied Mechanics and Engineering* 293 (2015), pp. 431–461.

[97] Matthias Heil. “An efficient solver for the fully coupled solution of large-displacement fluid–structure interaction problems”. In: *Computer Methods in Applied Mechanics and Engineering* 193.1-2 (2004), pp. 1–23.

[98] Stefanie Heyden et al. “Material modeling of cardiac valve tissue: Experiments, constitutive analysis and numerical investigation”. In: *Journal of biomechanics* 48.16 (2015), pp. 4287–4296.

[99] Jeannette Hiromi Spühler and Johan Hoffman. “An interface-tracking unified continuum model for fluid-structure interaction with topology change and full-friction contact with application to aortic valves”. In: *International Journal for Numerical Methods in Engineering* 122.19 (2021), pp. 5258–5278.

[100] C.W. Hirt, A.A. Amsden, and J.L. Cook. “An arbitrary Lagrangian Eulerian computing method for all flow speeds”. In: *Journal of Computational Physics* 69 (1974), pp. 277–324.

[101] Gerhard A Holzapfel and Ray W Ogden. "Constitutive modelling of passive myocardium: a structurally based framework for material characterization". In: *Philosophical Transactions of the Royal Society A: Mathematical, Physical and Engineering Sciences* 367.1902 (2009), pp. 3445–3475.

[102] Ming-Chen Hsu et al. "Dynamic and fluid–structure interaction simulations of bioprosthetic heart valves using parametric design with T-splines and Fung-type material models". In: *Computational mechanics* 55.6 (2015), pp. 1211–1225.

[103] Ming-Chen Hsu et al. "Fluid–structure interaction analysis of bioprosthetic heart valves: significance of arterial wall deformation". In: *Computational mechanics* 54.4 (2014), pp. 1055–1071.

[104] Thomas J R Hughes and Gregory M Hulbert. "Space-time finite element methods for elastodynamics: formulations and error estimates". In: *Computer methods in applied mechanics and engineering* 66.3 (1988), pp. 339–363. DOI: 10.1016/0045-7825(88)90006-0.

[105] Mahmoud Ismail, Wolfgang A Wall, and Michael W Gee. "Adjoint-based inverse analysis of windkessel parameters for patient-specific vascular models". In: *Journal of Computational Physics* 244 (2013), pp. 113–130.

[106] Lucian Itu et al. "A parameter estimation framework for patient-specific hemodynamic computations". In: *Journal of Computational Physics* 281 (2015), pp. 316–333.

[107] Emily L Johnson et al. "Effects of membrane and flexural stiffnesses on aortic valve dynamics: Identifying the mechanics of leaflet flutter in thinner biological tissues". In: *Forces in Mechanics* 6 (2022), p. 100053.

[108] T. Jonsson, M. G. Larson, and K. Larsson. "Cut finite element methods for elliptic problems on multipatch parametric surfaces". In: *Computer Methods in Applied Mechanics and Engineering* 324 (2017), pp. 366–394.

[109] D. Kamensky et al. "An immersogeometric variational framework for fluid–structure interaction: Application to bioprosthetic heart valves". In: *Computer Methods in Applied Mechanics and Engineering* 284 (2015), pp. 1005–1053. DOI: https://doi.org/10.1016/j.cma.2014.10.040. URL: https://www.sciencedirect.com/science/article/pii/S0045782514004101.

[110] Soonpil Kang, JaeHyuk Kwack, and Arif Masud. "Variational coupling of non-matching discretizations across finitely deforming fluid–structure interfaces". In: *International Journal for Numerical Methods in Fluids* 94.6 (2022), pp. 678–718.

[111] Elias Karabelas et al. “Global Sensitivity Analysis of Four Chamber Heart Hemodynamics Using Surrogate Models”. In: *IEEE Transactions on Biomedical Engineering* (2022).

[112] S. Katayama et al. “The sinus of Valsalva relieves abnormal stress on aortic valve leaflets by facilitating smooth closure”. In: *The Journal of thoracic and cardiovascular surgery* 136.6 (2008), pp. 1528–1535.

[113] Carl T Kelley. *Iterative methods for linear and nonlinear equations*. SIAM, 1995.

[114] SC Kelly and MJ O’rourke. “A two-system, single-analysis, fluid—structure interaction technique for modelling abdominal aortic aneurysms”. In: *Proceedings of the Institution of Mechanical Engineers, Part H: Journal of Engineering in Medicine* 224.8 (2010), pp. 955–969.

[115] Hyunggun Kim et al. “Dynamic simulation of bioprosthetic heart valves using a stress resultant shell model”. In: *Annals of biomedical engineering* 36.2 (2008), pp. 262–275.

[116] Woojin Kim and Haecheon Choi. “Immersed boundary methods for fluid-structure interaction: A review”. In: *International Journal of Heat and Fluid Flow* 75 (2019), pp. 301–309.

[117] Araz R Kivi et al. “Fluid structure interaction modelling of aortic valve stenosis: effects of valve calcification on coronary artery flow and aortic root hemodynamics”. In: *Computer Methods and Programs in Biomedicine* 196 (2020), p. 105647.

[118] Ulrich Küttler and Wolfgang A Wall. “Fixed-point fluid–structure interaction solvers with dynamic relaxation”. In: *Computational mechanics* 43.1 (2008), pp. 61–72.

[119] Y. G. Lai, K. B. Chandran, and J. Lemmon. “A numerical simulation of mechanical heart valve closure fluid dynamics”. In: *Journal of Biomechanics* 35(7) (2002), pp. 881–892.

[120] Jonas Lantz, Johan Renner, and Matts Karlsson. “Wall shear stress in a subject specific human aorta—influence of fluid-structure interaction”. In: *International Journal of Applied Mechanics* 3.04 (2011), pp. 759–778.

[121] T. B. Le and F. Sotiropoulos. “Fluid–structure interaction of an aortic heart valve prosthesis driven by an animated anatomic left ventricle”. In: *Journal of Computational Physics* 244 (2013), pp. 41–62.

[122] Xujing Li, Xiaodi Zhang, and Xinxin Zhou. “High order interface-penalty finite element methods for elliptic interface problems with Robin jump conditions”. In: *Computer Methods in Applied Mechanics and Engineering* 390 (2022), p. 114505.

[123] Zhilin Li, Tao Lin, and Xiaohui Wu. "New Cartesian grid methods for interface problems using the finite element formulation". In: *Numerische Mathematik* 96.1 (2003), pp. 61–98.

[124] Alexey Liogky, Pavel Karavaikin, and Victoria Salamatova. "Impact of material stiffness and anisotropy on coaptation characteristics for aortic valve cusps reconstructed from pericardium". In: *Mathematics* 9.18 (2021), p. 2193.

[125] Dan Lior et al. "Semi-Automated Construction of Patient-Specific Aortic Valves from Computed Tomography Images". In: *Annals of Biomedical Engineering* (2022), pp. 1–11.

[126] Konstantin Lipnikov, Danail Vassilev, and Ivan Yotov. "Discontinuous Galerkin and mimetic finite difference methods for coupled Stokes–Darcy flows on polygonal and polyhedral grids". In: *Numerische Mathematik* 126.2 (2014), pp. 321–360.

[127] Bin Liu and Danielle Tan. "A Nitsche stabilized finite element method for embedded interfaces: Application to fluid-structure interaction and rigid-body contact". In: *Journal of Computational Physics* 413 (2020), p. 109461.

[128] Minliang Liu, Liang Liang, and Wei Sun. "Estimation of in vivo constitutive parameters of the aortic wall using a machine learning approach". In: *Computer methods in applied mechanics and engineering* 347 (2019), pp. 201–217.

[129] W. K. Liu et al. "Immersed finite element method and its applications to biological systems". In: *Computer Methods in Applied Mechanics and Engineering* 195.13 (2006), pp. 1722–1749.

[130] Raoul van Loon, Patrick D Anderson, and Frans N van de Vosse. "A fluid–structure interaction method with solid-rigid contact for heart valve dynamics". In: *Journal of computational physics* 217.2 (2006), pp. 806–823.

[131] Giulia Luraghi et al. "Does clinical data quality affect fluid-structure interaction simulations of patient-specific stenotic aortic valve models?" In: *Journal of Biomechanics* 94 (2019), pp. 202–210.

[132] Giulia Luraghi et al. "On the modeling of patient-specific transcatheter aortic valve replacement: a fluid–structure interaction approach". In: *Cardiovascular engineering and technology* 10.3 (2019), pp. 437–455.

[133] Alex Main and Guglielmo Scovazzi. "The shifted boundary method for embedded domain computations. Part I: Poisson and Stokes problems". In: *Journal of Computational Physics* 372 (2018), pp. 972–995.

[134] Alex Main and Guglielmo Scovazzi. “The shifted boundary method for embedded domain computations. Part II: Linear advection–diffusion and incompressible Navier–Stokes equations”. In: *Journal of Computational Physics* 372 (2018), pp. 996–1026.

[135] A Cristiano I Malossi and Jean Bonnemain. “Numerical comparison and calibration of geometrical multiscale models for the simulation of arterial flows”. In: *Cardiovascular Engineering and Technology* 4.4 (2013), pp. 440–463.

[136] Tommaso Mansi et al. “An integrated framework for finite-element modeling of mitral valve biomechanics from medical images: application to MitralClip intervention planning”. In: *Medical image analysis* 16.7 (2012), pp. 1330–1346.

[137] Gil Marom. “Numerical methods for fluid–structure interaction models of aortic valves”. In: *Archives of Computational Methods in Engineering* 22.4 (2015), pp. 595–620.

[138] Gil Marom et al. “A fluid–structure interaction model of the aortic valve with coaptation and compliant aortic root”. In: *Medical & biological engineering & computing* 50.2 (2012), pp. 173–182.

[139] André Massing et al. “A Nitsche-based cut finite element method for a fluid-structure interaction problem”. In: *Communications in Applied Mathematics and Computational Science* 10.2 (2015), pp. 97–120.

[140] Ursula M Mayer et al. “3D fluid–structure-contact interaction based on a combined XFEM FSI and dual mortar contact approach”. In: *Computational Mechanics* 46.1 (2010), pp. 53–67.

[141] Rajat Mittal and Gianluca Iaccarino. “Immersed boundary methods”. In: *Annu. Rev. Fluid Mech.* 37 (2005), pp. 239–261.

[142] Philippe Moireau et al. “External tissue support and fluid–structure simulation in blood flows”. In: *Biomechanics and modeling in mechanobiology* 11.1 (2012), pp. 1–18.

[143] Philippe Moireau et al. “Sequential identification of boundary support parameters in a fluid-structure vascular model using patient image data”. In: *Biomechanics and modeling in mechanobiology* 12.3 (2013), pp. 475–496.

[144] Y. S. Morsi et al. “Transient fluid–structure coupling for simulation of a trileaflet heart valve using weak coupling”. In: *Journal of artificial organs* 10.2 (2007), pp. 96–103.

[145] Maria Giuseppina Chiara Nestola et al. “An immersed boundary method for fluid-structure interaction based on variational transfer”. In: *Journal of computational physics* 398 (2019), p. 108884.

[146] Cosmin-Ioan Nita et al. "Personalized Pre-and Post-Operative Hemodynamic Assessment of Aortic Coarctation from 3D Rotational Angiography". In: *Cardiovascular Engineering and Technology* 13.1 (2022), pp. 14–40.

[147] F. Nobile. "Numerical approximation of fluid-structure interaction problems with application to haemodynamics". Thesis n° 2458. PhD thesis. École Polytechnique Fédérale de Lausanne, 2001.

[148] Fabio Nobile, Matteo Pozzoli, and Christian Vergara. "Inexact accurate partitioned algorithms for fluid–structure interaction problems with finite elasticity in haemodynamics". In: *Journal of Computational Physics* 273 (2014), pp. 598–617.

[149] Fabio Nobile, Matteo Pozzoli, and Christian Vergara. "Time accurate partitioned algorithms for the solution of fluid–structure interaction problems in haemodynamics". In: *Computers & Fluids* 86 (2013), pp. 470–482.

[150] Fabio Nobile and Christian Vergara. "An effective fluid-structure interaction formulation for vascular dynamics by generalized Robin conditions". In: *SIAM Journal on Scientific Computing* 30.2 (2008), pp. 731–763.

[151] Salvatore Pasta et al. "Computer modeling for the prediction of thoracic aortic stent graft collapse". In: *Journal of vascular surgery* 57.5 (2013), pp. 1353–1361.

[152] Joaquim Peiró and Alessandro Veneziani. "Reduced models of the cardiovascular system". In: *Cardiovascular mathematics*. Springer, 2009, pp. 347–394.

[153] Mauro Perego, Alessandro Veneziani, and Christian Vergara. "A variational approach for estimating the compliance of the cardiovascular tissue: An inverse fluid-structure interaction problem". In: *SIAM journal on scientific computing* 33.3 (2011), pp. 1181–1211.

[154] Charles S Peskin. "Flow patterns around heart valves: A numerical method". In: *Journal of Computational Physics* 10.2 (1972), pp. 252–271. ISSN: 0021-9991.

[155] Ramón Pons et al. "Fluid–structure interaction simulations outperform computational fluid dynamics in the description of thoracic aorta haemodynamics and in the differentiation of progressive dilation in Marfan syndrome patients". In: *Royal Society open science* 7.2 (2020), p. 191752.

[156] Yonghui Qiao et al. "A primary computational fluid dynamics study of pre-and post-TEVAR with intentional left subclavian artery coverage in a type B aortic dissection". In: *Journal of Biomechanical Engineering* 141.11 (2019).

[157] Yonghui Qiao et al. "Numerical simulation of two-phase non-Newtonian blood flow with fluid-structure interaction in aortic dissection". In: *Computer methods in biomechanics and biomedical engineering* 22.6 (2019), pp. 620–630.

[158] Alfio Quarteroni, Andrea Manzoni, and Christian Vergara. "The cardiovascular system: mathematical modelling, numerical algorithms and clinical applications". In: *Acta Numerica* 26 (2017), pp. 365–590.

[159] Alfio Quarteroni and Alberto Valli. *Numerical approximation of partial differential equations*. Vol. 23. Springer Science & Business Media, 2008.

[160] Alfio Quarteroni, Alessandro Veneziani, and Christian Vergara. "Geometric multiscale modeling of the cardiovascular system, between theory and practice". In: *Computer Methods in Applied Mechanics and Engineering* 302 (2016), pp. 193–252.

[161] ML Raghavan, Baoshun Ma, Mark Fillinger, et al. "Non-invasive determination of zero-pressure geometry of arterial aneurysms". In: *Annals of biomedical engineering* 34.9 (2006), pp. 1414–1419.

[162] Th Richter and Th Wick. "Finite elements for fluid–structure interaction in ALE and fully Eulerian coordinates". In: *Computer Methods in Applied Mechanics and Engineering* 199.41-44 (2010), pp. 2633–2642.

[163] Rodrigo M Romarowski et al. "Patient-specific CFD modelling in the thoracic aorta with PC-MRI–based boundary conditions: A least-square three-element Windkessel approach". In: *International journal for numerical methods in biomedical engineering* 34.11 (2018), e3134.

[164] Yongyuth Sahasakul et al. "Age-related changes in aortic and mitral valve thickness: implications for two-dimensional echocardiography based on an autopsy study of 200 normal human hearts". In: *The American journal of cardiology* 62.7 (1988), pp. 424–430.

[165] Simone Saitta et al. "Evaluation of 4D flow MRI-based non-invasive pressure assessment in aortic coarctations". In: *Journal of biomechanics* 94 (2019), pp. 13–21.

[166] Alfonso Santiago et al. "Fully coupled fluid-electro-mechanical model of the human heart for supercomputers". In: *International journal for numerical methods in biomedical engineering* 34.12 (2018), e3140.

[167] B. Schott and W. A. Wall. "A new face-oriented stabilized XFEM approach for 2D and 3D incompressible Navier-Stokes equations". In: *Computer Methods in Applied Mechanics and Engineering* 276 (2014), pp. 233–265. ISSN: 0045-7825. DOI: http://dx.doi.org/10.1016/j.cma.2014.02.014. URL: http://www.sciencedirect.com/science/article/pii/S0045782514000711.

[168] Anyastassia Seboldt and Martina Bukač. "A non-iterative domain decomposition method for the interaction between a fluid and a thick structure". In: *Numerical Methods for Partial Differential Equations* 37.4 (2021), pp. 2803–2832.

[169] Jung-Hee Seo et al. "Flow physics of normal and abnormal bioprosthetic aortic valves". In: *International Journal of Heat and Fluid Flow* 86 (2020), p. 108740.

[170] Daniel A Serino et al. "A stable added-mass partitioned (AMP) algorithm for elastic solids and incompressible flow: Model problem analysis". In: *SIAM Journal on Scientific Computing* 41.4 (2019), A2464–A2484.

[171] Alexander Shamanskiy and Bernd Simeon. "Mesh moving techniques in fluid-structure interaction: robustness, accumulated distortion and computational efficiency". In: *Computational Mechanics* 67.2 (2021), pp. 583–600.

[172] Fotis Sotiropoulos and Xiaolei Yang. "Immersed boundary methods for simulating fluid–structure interaction". In: *Progress in Aerospace Sciences* 65 (2014), pp. 1–21.

[173] Thomas Spenke, Norbert Hosters, and Marek Behr. "A multi-vector interface quasi-Newton method with linear complexity for partitioned fluid–structure interaction". In: *Computer Methods in Applied Mechanics and Engineering* 361 (2020), p. 112810.

[174] Thomas Spenke, Michel Make, and Norbert Hosters. "A Robin-Neumann scheme with quasi-Newton accelerationfor partitioned fluid-structure interaction". In: *Int J Numer Methods Eng* (2022). DOI: 10.1002/nme.7151.

[175] Keith Stein, Tayfun Tezduyar, and Richard Benney. "Mesh moving techniques for fluid-structure interactions with large displacements". In: *J. Appl. Mech.* 70.1 (2003), pp. 58–63.

[176] J. M. A. Stijnen et al. "Evaluation of a fictitious domain method for predicting dynamic response of mechanical heart valves". In: *Journal of Fluids and Structures* 19.6 (2004), pp. 835–850.

[177] Seiryo Sugiura et al. "UT-Heart: A Finite Element Model Designed for the Multiscale and Multiphysics Integration of our Knowledge on the Human Heart". In: *Computational Systems Biology in Medicine and Biotechnology*. Springer, 2022, pp. 221–245.

[178] Kenji Takizawa et al. "Heart valve flow computation with the Space–Time Slip Interface Topology Change (ST-SI-TC) method and Isogeometric Analysis (IGA)". In: *Biomedical Technology*. Springer, 2018, pp. 77–99. DOI: 10.1007/978-3-319-59548-1_6.

[179] Tayfun E Tezduyar and Sunil Sathe. "Modelling of fluid–structure interactions with the space–time finite elements: solution techniques". In: *International Journal for Numerical Methods in Fluids* 54.6-8 (2007), pp. 855–900. DOI: 10.1016/0045-7825(88)90006-0.

[180] Tayfun E Tezduyar, Sunil Sathe, and Keith Stein. "Solution techniques for the fully discretized equations in computation of fluid–structure interactions with the space–time formulations". In: *Computer Methods in Applied Mechanics and Engineering* 195.41-43 (2006), pp. 5743–5753.

[181] Alexandre This et al. "A pipeline for image based intracardiac CFD modeling and application to the evaluation of the PISA method". In: *Computer Methods in Applied Mechanics and Engineering* 358 (2020), p. 112627.

[182] Alexandre This et al. "Augmented resistive immersed surfaces valve model for the simulation of cardiac hemodynamics with isovolumetric phases". In: *International journal for numerical methods in biomedical engineering* 36.3 (2020), e3223.

[183] Yuri Vassilevski, Alexey Liogky, and Victoria Salamatova. "Application of Hyperelastic Nodal Force Method to Evaluation of Aortic Valve Cusps Coaptation: Thin Shell vs. Membrane Formulations". In: *Mathematics* 9.12 (2021), p. 1450.

[184] Marcel van't Veer et al. "Biomechanical properties of abdominal aortic aneurysms assessed by simultaneously measured pressure and volume changes in humans". In: *Journal of vascular surgery* 48.6 (2008), pp. 1401–1407.

[185] Christian Vergara and Stefano Zonca. "Extended finite elements method for fluid-structure interaction with an immersed thick non-linear structure". In: *Mathematical and Numerical Modeling of the Cardiovascular System and Applications*. Springer, 2018, pp. 209–243.

[186] Roberto Verzicco. "Immersed Boundary Methods: Historical Perspective and Future Outlook". In: *Annual Review of Fluid Mechanics* 55 (2023).

[187] Irene E Vignon-Clementel et al. "Outflow boundary conditions for three-dimensional finite element modeling of blood flow and pressure in arteries". In: *Computer methods in applied mechanics and engineering* 195.29-32 (2006), pp. 3776–3796.

[188] Francesco Viola, Valentina Meschini, and Roberto Verzicco. "Fluid–Structure-Electrophysiology interaction (FSEI) in the left-heart: a multi-way coupled computational model". In: *European Journal of Mechanics-B/Fluids* 79 (2020), pp. 212–232.

[189] Francesco Viola et al. "GPU accelerated digital twins of the human heart open new routes for cardiovascular research". In: (2022).

[190] Charalambos Vlachopoulos, Michael O'Rourke, and Wilmer W Nichols. *McDonald's blood flow in arteries: theoretical, experimental and clinical principles*. CRC press, 2011.

[191] Emiliano Votta et al. "Toward patient-specific simulations of cardiac valves: state-of-the-art and future directions". In: *Journal of biomechanics* 46.2 (2013), pp. 217–228.

[192] Jingyang Wang, Chunhua Zhou, and Junqiang Ai. "A hybrid immersed-boundary/body-fitted-grid method and its application to simulating heart valve flows". In: *International Journal for Numerical Methods in Fluids* 94.12 (2022), pp. 1996–2019.

[193] Xiaodong Wang and Wing Kam Liu. "Extended immersed boundary method using FEM and RKPM". In: *Computer Methods in Applied Mechanics and Engineering* 193.12-14 (2004), pp. 1305–1321.

[194] E. J. Weinberg et al. "Hemodynamic environments from opposing sides of human aortic valve leaflets evoke distinct endothelial phenotypes in vitro". In: *Cardiovascular engineering* 10.1 (2010), pp. 5–11.

[195] Eli J Weinberg, Frederick J Schoen, and Mohammad RK Mofrad. "A computational model of aging and calcification in the aortic heart valve". In: *PLoS One* 4.6 (2009), e5960.

[196] Nico Westerhof, Jan-Willem Lankhaar, and Berend E Westerhof. "The arterial windkessel". In: *Medical & biological engineering & computing* 47.2 (2009), pp. 131–141.

[197] Michael CH Wu et al. "Immersogeometric fluid–structure interaction modeling and simulation of transcatheter aortic valve replacement". In: *Computer Methods in Applied Mechanics and Engineering* 357 (2019), p. 112556.

[198] Yuqi Wu and Xiao-Chuan Cai. "A fully implicit domain decomposition based ALE framework for three-dimensional fluid–structure interaction with application in blood flow computation". In: *Journal of Computational Physics* 258 (2014), pp. 524–537.

[199] Yifan Yang et al. "An ALE approach to mechano-chemical processes in fluid–structure interactions". In: *International Journal for Numerical Methods in Fluids* 84.4 (2017), pp. 199–220.

[200] Yue Yu, Hyoungsu Baek, and George Em Karniadakis. "Generalized fictitious methods for fluid–structure interactions: analysis and simulations". In: *Journal of Computational Physics* 245 (2013), pp. 317–346.

[201] L. T. Zhang and M. Gay. "Immersed finite element method for fluid-structure interactions". In: *Journal of Fluids and Structures* 23.6 (2007), pp. 839–857.

[202] L. T. Zhang et al. “Immersed finite element method”. In: *Computer Methods in Applied Mechanics and Engineering* 193.21 (2004), pp. 2051–2067.

[203] Xiaodi Zhang. “High order interface-penalty finite element methods for elasticity interface problems in 3D”. In: *Computers & Mathematics with Applications* 114 (2022), pp. 161–170.

[204] Chi Zhu, Jung-Hee Seo, and Rajat Mittal. “Computational Modeling of Aortic Stenosis With a Reduced Degree-of-Freedom Fluid-Structure Interaction Valve Model”. In: *Journal of Biomechanical Engineering* 144.3 (2022).

[205] Alberto Zingaro et al. “A geometric multiscale model for the numerical simulation of blood flow in the human left heart”. In: *Discrete and Continuous Dynamical Systems-S* (2022).

[206] Stefano Zonca, Paola F Antonietti, Christian Vergara, et al. “A polygonal discontinuous Galerkin formulation for contact mechanics in fluid-structure interaction problems”. In: *Commun. Comput. Phys.* 30.1 (2021), pp. 1–33.

[207] Stefano Zonca, Christian Vergara, and Luca Formaggia. “An unfitted formulation for the interaction of an incompressible fluid with a thick structure via an XFEM/DG approach”. In: *SIAM Journal on Scientific Computing* 40.1 (2018), B59–B84.

[208] Rubén Zorrilla et al. “An embedded Finite Element framework for the resolution of strongly coupled Fluid–Structure Interaction problems. Application to volumetric and membrane-like structures”. In: *Computer Methods in Applied Mechanics and Engineering* 368 (2020), p. 113179.

## MOX Technical Reports, last issues

Dipartimento di Matematica
Politecnico di Milano, Via Bonardi 9 - 20133 Milano (Italy)

**04/2023** Quarteroni, A.; Dede', L.; Regazzoni, F.; Vergara, C.
*A mathematical model of the human heart suitable to address clinical problems*

**02/2023** Boon, W. M.; Fumagalli, A.; Scotti, A.
*Mixed and multipoint finite element methods for rotation-based poroelasticity*

**03/2023** Africa, P.C.; Perotto, S.; de Falco, C.
*Scalable Recovery-based Adaptation on Quadtree Meshes for Advection-Diffusion-Reaction Problems*

**01/2023** Zingaro, A.; Bucelli, M.; Piersanti, R.; Regazzoni, F.; Dede', L.; Quarteroni, A.
*An electromechanics-driven fluid dynamics model for the simulation of the whole human heart*

**82/2022** Ciaramella, G.; Gander, M.; Van Criekingen, S.; Vanzan, T.
*A PETSc Parallel Implementation of Substructured One- and Two-level Schwarz Methods*

**81/2022** Bonizzoni, F.; Hauck, M.; Peterseim, D.
*A reduced basis super-localized orthogonal decomposition for reaction-convection-diffusion problems*

**84/2022** Ciaramella, G.; Gambarini, M.; Miglio, E.
*A preconditioner for free-surface hydrodynamics BEM*

**85/2022** Lurani Cernuschi , A.; Masci, C.; Corso, F.; Muccini, C.; Ceccarelli, D.; San Raffaele Hospital Galli, L.; Ieva, F.; Paganoni, A.M.; Castagna, A.
*A neural network approach to survival analysis for modelling time to cardiovascular diseases in HIV patients with longitudinal observations*

**83/2022** Ciaramella, G.; Gander, M.; Mazzieri, I.
*Unmapped tent pitching schemes by waveform relaxation*

**80/2022** Balduzzi, G.; Bonizzoni, F.; Tamellini, L.
*Uncertainty quantification in timber-like beams using sparse grids: theory and examples with off-the-shelf software utilization*